Modeling of methylene blue removal on Fe$_3$O$_4$ modified activated carbon with artificial neural network (ANN)

Esra Altintig, Tijen Över Özcelik, Zeynep Aydemir, Dilay Bozdag, Eren Kilic & Ayten Yılmaz Yalçıner

Published online: 17 Mar 2023.

Submit your article to this journal ⓒ

Article views: 234

View related articles ⓒ

View Crossmark data ⓒ

Taylor & Francis
Taylor & Francis Group

Check for updates

Modeling of methylene blue removal on Fe$_3$O$_4$ modified activated carbon with artificial neural network (ANN)

Esra Altintig[a], Tijen Över Özcelik[b], Zeynep Aydemir[c], Dilay Bozdag[b,d], Eren Kilic[e], and Ayten Yılmaz Yalçıner[b]

[a]Pamukova Vocational School, Sakarya University of Applied Sciences, Sakarya, Turkey; [b]Industrial Engineering Department, Engineering Faculty, Sakarya University, Sakarya, Turkey; [c]Faculty of Science, Sakarya University, Sakarya, Turkey; [d]Akcoat Advanced Chemical Coating Materials Industry and Trade Joint Stock Company, Sakarya, Turkey; [e]Ser Durable Consumer Goods Domestic and Foreign Trade Industry Inc., Kayseri, Turkey

ABSTRACT

In this study, AC/Fe$_3$O$_4$ adsorbent was first synthesized by modifying activated carbon with Fe$_3$O$_4$. The structure of the adsorbent was then characterized using analysis techniques specific surface area (BET), Scanning Electron Microscopy with Energy Dispersive X-ray Spectroscopy (SEM-EDX), and Fourier Transform Infrared Spectroscopy (FTIR). Equilibrium, thermodynamic and kinetic studies were carried out on the removal of methylene blue (MB) dyestuff from aqueous solutions AC/Fe$_3$O$_4$ adsorbent. The Langmuir maximum adsorption capacity of AC/Fe$_3$O$_4$ was 312.8 mg g^{-1}, and the best fitness was observed with the pseudo-second-order kinetics model, with an endothermic adsorption process. In the final stage of the study, the adsorption process of MB on AC/Fe$_3$O$_4$ was modeled using artificial neural network modeling (ANN). Considering the smallest mean square error (MSE), The backpropagation neural network was configured as a three-layer ANN with a tangent sigmoid transfer function (Tansig) at the hidden layer with 10 neurons, linear transfer function (Purelin) the at output layer and Levenberg-Marquardt backpropagation training algorithm (LMA). Input parameters included initial solution pH (2.0–9.0), amount (0.05–0.5 g L^{-1}), temperature (298–318 K), contact time (5–180 min), and concentration (50–500 mg L^{-1}). The effect of each parameter on the removal and adsorption percentages was evaluated. The performance of the ANN model was adjusted by changing parameters such as the number of neurons in the middle layer, the number of inputs, and the learning coefficient. The mean absolute percentage error (MAPE) was used to evaluate the model's accuracy for the removal and adsorption percentage output parameters. The absolute fraction of variance (R^2) values were 99.83, 99.36, and 98.26% for the dyestuff training, validation, and test sets, respectively.

NOVELTY STATEMENT

The aspect of the study, which is expected to contribute to the literature, firstly, we performed the characterization process of the iron-coated activated carbon with analytical measurements. Then, we verified the adsorption process by performing pH effect, equilibrium, kinetic and thermodynamic studies. Our primary goal is to statistically demonstrate that efficiency estimation can be made in a shorter time with smart methods, especially by comparing real experimental results with ANN estimation results obtained from modern artificial intelligence techniques. We believe that this aim will provide a different perspective to the literature in terms of obtaining results with minimum cost and effort for these processes with high accuracy and consistency.

GRAPHICAL ABSTRACT
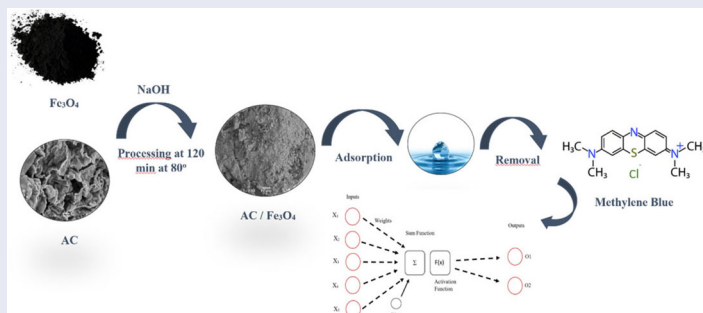
Introduction

Chemical pollutants released directly or indirectly into the environment, especially from industrial facilities, adversely affect water systems (Mahmoodi et al. 2006; Mahmoodi, Arami, et al. 2007; Mahmoodi, Limaee, et al. 2007; Hamd et al. 2021). Among these industrial sectors, the textile sector is one of the most rapidly developing sectors in Turkey and throughout the world, and contributes a large share to the Turkish economy (Mahmoodi et al. 2014; Yaseen and Scholz 2019; Ghaedi and Vafaei 2017). However, the unwanted dyestuffs and chemicals that the textile industry industry produces as biproducts spreads to the environment cause environmental pollution. The dyes consists of soluble organic compounds, in particular those classified as reactive, direct, basic, and acidic (Mahmoodi, Arami, et al. 2007; Gharanjig et al. 2008). They exhibit a high solubility in water, making it difficult to remove them by conventional methods (Hamd et al. 2021). One of the properties of such dyes is the ability to impart color to a particular substrate due to the presence of chromophoric groups in their molecular structure (Shamey and Zhao 2014). However, this ability to fix the color of the material is related to the auxotrophic groups, which are polar and can bind to the polar groups of the textile fibers. Dyes are one of the most dangerous industrial pollutants in that can cause skin diseases and allergies and provoke cancer and mutation in humans (Mahmoodi and Arami 2009; Rahdar et al. 2021). The accumulation of such dyes in organisms create toxic and carcinogenic products, and this causes the direct destruction of aquatic organisms. Moreover, hampering light transmittance causes significant environmental issues because this reduces photosynthetic activity in the aquatic life. Therefore, it is vital to remove dyestuffs from industrial wastewater (Khedr et al. 2013). Millions of tons of dyestuffs are released from various textile industries every year, (Boguniewicz-Zablocka et al. 2020; Hynes et al. 2020) and the discharge of large amounts of colored dyestuffs and pigments poses a real environmental threat (Fernandes et al. 2020; Mokhtari et al. 2020). Colorants enter the water body and, due to their complex molecular structure do not decompose readily. This affects environmental pollution (Mahmoodi 2013b; Jawad et al. 2022). Water pollution is one of the consequences of this effect, with 17–20% of water pollution being due to textile dyeing and processing (Yuan et al. 2017; Hussain et al. 2022). One of the popular thiazine redox cationic dyes that is environmentally persistent, toxic, carcinogenic, and mutagenic is methylene blue (MB) dye (Teow et al. 2019). It is widely applied as a synthetic dye for dyeing fabrics in the clothing and textile industries and dyeing paper and leather. In line with the magnitude of industrial use, large quantities of MB dye-containing wastewater are discharged into groundwater and surface waters. At doses greater than 5 mg kg^{-1}, the monoamine oxidase inhibitory properties of MB dye can cause fatal serotonin toxicity in humans, as well as a threat to fauna in the aquatic ecosystem (Oladoye et al. 2022). Although MB dyestuff is not considered acutely toxic, it has many harmful effects on human health when humans are exposed to excessive amounts. For example, inhalation can cause short-term, rapid, and difficult breathing (Rehman et al. 2012; Balarak et al. 2015). Ingestion with food causes a burning sensation and sometimes, results in vomiting, diarrhea, nausea, gastritis, abdominal and chest pain, severe headache, mental confusion, excessive sweating, urinary tract infection, and methemoglobin anemia in severe cases (Sen et al. 2011; Abdurrahman et al. 2013). Therefore, the removal of MB from the effluent is essential due to its harmful impacts (Rehman et al. 2012). Many different methods can be used to remove such dyestuffs from water, including biological treatment, precipitation, ion exchange (Joseph et al. 2020), filtration (Ahmad et al. 2018), chemical oxidation (Rajkumar et al. 2007), adsorption (Mahmoodi et al. 2007; Altintig, Kabadayi, et al. 2022; Pandey et al. 2023), ozone treatment (Bianco et al. 2020), advanced oxidation (Dehghani and Mahdavi 2015). Biological dye removal methods incorporate some form of the living organism in its process. The use of enzymes to remove dye is becoming common these days as it is believed a range of biological dye removal methods are the cheapest as well as safest methods of remedying the situation (Karami et al. 2017). Since these method deal with living things, their major disadvantage is its growth rate (Katheresan et al. 2018). System instability is common in biological dye removal processes in that predicting its growth rate and reactions can be tricky at times (Sharafi et al. 2015). However, these processes are expensive to operate are relatively inefficient and generate large volumes of sludge as a result of the processes. The most preferred method is the adsorption method in terms of ease of use and cost (Mahmoodi and Shourijeh 2015; Sharafi et al. 2015; Altintig, Kabadayi, et al. 2022). In this process, natural or modified minerals such as bentonite, zeolite, red mud, montmorillonite, pumice, and activated carbon (AC) obtained from agricultural wastes are used (Shayesteh et al. 2016). Among the various adsorbents used, AC material is frequently applied for wastewater decontamination due to its porous structure, and its functional properties such as easy design and modification (Qu et al. 2019). There are many studies in the literature on the preparation of AC from different agricultural wastes as a low-cost and renewable precursor. In this context, various agricultural wastes and by-products such as coconut shells (Dibi et al. 2021), coffee shells (Altintig et al. 2021), dragon fruit shells (Jawad et al., 2021), Fruit peel (Yousef et al. 2022), carrot juice pulp and pomegranate peel (Suhaimi et al. 2022), cherry kernels (Angin 2014), soy meal hull (Mahmoodi 2014b), Mango Peels and Seeds Wastes (Razali et al. 2022) have been successfully used for the preparation of porous AC with potential application for MB removal. However, the most critical problem in using AC as an adsorbent is the removal of carbon from the solution after the adsorption process, and using costly and time-consuming methods such as filtration (D'Cruz et al. 2020). In the literature, purified lignocellulosic biomass wastes supported by FeCl$_3$/Zn (NO$_3$)$_2$ are used in dye removal. It takes the form

of an effective composite. In recent studies, AC has been modified with the addition of metal oxides due to its reusability and high surface area. This modification is also very advantageous for removing organic contaminants from aqueous solutions (Agarwal *et al.* 2016). Recently, iron-enriched AC has been used as an alternative due to its advantage over other AC enrichment methods (Saleh *et al.* 2017). Various applications for removal of organic pollutants with materials coated with metal oxides on the AC surface are available. Metal oxides are added to the adsorbent surfaces *via* chemical modification that lead to an increase in the adsorption capacity of natural adsorbents (Mahmoodi *et al.* 2006). Chemical modification is done using the precipitation method, and as a result, adsorption occurs over a wide range of pH values and lower concentrations (Kant *et al.* 2014). Magnetic adsorbents are an especially attractive solution for metallic and organic aqueous contaminants because of the simple magnetic separation process (Mahmoodi *et al.* 2006). In recent years, different studies on metal oxide adsorbents have become very popular in the literature. In a study by Rahdar *et al.* MgO-supported Fe–Co–Mn nanoparticles were synthesized and used as adsorbents for successful removal of RhB dye from aqueous media (Rahdar *et al.* 2019). In the study of Ahmadi *et al.* Nd_2O_3 nanoparticles were synthesized and characterized by means of XRD, FTIR, and SEM. The main aim of their research was to tune/model and optimize the removal of Acid Blue 92 (AB92) dye from synthetic wastes (aqueous solutions) using the adsorption process based on Nd_2O_3 nanoparticles. Central compound design based on response surface methodology was applied to optimize the adsorption conditions. They investigated the effects of pH (3–9), adsorbent dose (0.1–1 g L^{-1}), initial concentration of AB92 (100–300 mg L^{-1}), and contact time (10–100 min) on the adsorption process (Ahmadi *et al.* 2020). In the year 2022, Pandey and his friends in their study, magnetic iron oxide mineralization in place of iron ions through the hydrogel matrix (IO) integrated with Locust gum-cl-hydrogel nanocomposites of polyacrylonitrile (LBG-cl-PAN/IONP) basic method for the design and synthesis is presented. LBG-cl-PAN/IONP NC was used as an adsorbent to adsorb MB and MV dyes. In the study, a large number of study parameters were investigated, including the amount of adsorbent, contact time, pH, temperature, dye concentration, and co-existing ion concentration. Due to their properties, these materials are said to be promising in supercapacitors and environmental cleaning processes (Pandey, Son, and Kang *et al.* 2022). In the study of Mahmoodi (2015), a zinc ferrite nanoparticle was synthesized and its surface was modified using SDS. The modified nanoparticle was used as an adsorbent. Dyes were extracted from single and triple systems using ZFN–SDS (Mahmoodi 2015). In the year 2022, Pandey *et al.* in their study, a basic method for designing and synthesizing magnetic iron oxide (IO)-integrated locust bean gum-cl-polyacrylonitrile hydrogel nanocomposites (LBG-cl-PAN/IONP) *via in situ* mineralization of iron ions in a hydrogel matrix is presented. LBG-cl-PAN/IONP HNC is expressed as a promising sorbent or

composite material for removing toxic dyes from water and is therefore applicable to improving water and wastewater treatment technology. Due to their properties, these materials are said to be promising in supercapacitors and environmental cleaning processes (Pandey, Son, and Kang 2022). In their 2019 study, Pandey *et al.* focused on HNCs as sustainable materials and investigated the impact of nanoparticles used the n hydrogel, with a potential future perspective to overcome the current global water pollution crisis (Pandey, Son, and Kang 2022). Abdulhameed *et al.*, in their study in 2022, applied an environmentally friendly and efficient microalgae adsorbent (MAG) for the removal of crystal violet and methylene blue dyes from aqueous solutions. Multivariate modeling and optimization of CV and MB dyes removal were applied to MAG *via* the Box-Behnken design (BBD) based on three variables: MAG dosage, initial pH, and adsorption time studied. The maximum adsorption capacity of MAG produced from the Langmuir equation was calculated as 243.0 mg g^{-1} for CV and 297.1 mg g^{-1} for MB (Abdulhameed *et al.* 2022). In his study in 2019, Jawad carbonized the rubber (*Hevea brasiliensis*) seed coat, which is an agricultural waste, with H_2SO_4 as a potential biochar adsorbent for MB adsorption from aqueous solution with one-step liquid phase activation. Equilibrium data correlated well with the Langmuir isotherm compared to the Freundlich and Temkin models, and the maximum adsorption capacity of CRSS for MB adsorption, q_{max}, was 208.3 mg g^{-1} at optimum pH 8 and 303 K temperature. All stated results revealed that CRSS can be used appropriately for the removal of MB from an aqueous solution (Jawad 2018). Jawad *et al.* obtained a potential biochar adsorbent for MB adsorption from an aqueous solution by activating rubber (*Hevea brasiliensis*) leaf with H_2SO_4 in 2018. Various analytical techniques were used for its characterization. By performing equilibrium, kinetic and thermodynamic studies, they demonstrated that ATRL could be used in a viable manner for the removal of MB from an aqueous solution (Jawad *et al.* 2018).

Advances in computer technologies in recent years have increased the interest in studies on artificial intelligence. Observing the information-processing principles of humans and imitating the functioning of biological nervous systems are the main goals of artificial intelligence research (Zeng *et al.* 2016). Artificial intelligence research (ANNs), on the other hand, is a logical programming form developed by imitating the working mechanism of the human brain. ANN is a learning algorithm that can work with the human brain in the computer environment, make decisions, and reach the result by using the available data in case of insufficient data (Qi *et al.* 2020). Mathematical computational models are ANN, an input layer, hidden layers, and an output layer. They are often used to model complex systems and find relationships between inputs and outputs. The model considered in this work is represented by a three-layer feed-forward multilayer perceptron ANNs. The version used in this work is represented by a variant proposed, the main reason for its selection being good performance, flexibility, and easiness of use (Sharafi *et al.* 2019). ANNs are now used in many areas of science and engineering and are considered a promising

tool because of their simplicity toward simulation, prediction, and modeling. The advantages of ANN are that the mathematical description of the phenomena involved in the process is not required; less time is required for model development than the traditional mathematical models and prediction ability, with limited numbers of experiments (Arabameri et al. 2015). The percent removal is an important parameter for the adsorption process, but these data are quite difficult due to the time-consuming nature of data collection. Inspired by biological neural processes, an ANN can be applied to the adsorption process (Chowdhury and Saha 2013). Modeling and simulation of the adsorption process are very important as they can predict the adsorption process and complex functional relationships (Ghaedi and Vafaei 2017). With kinetic modeling, it is possible to determine the step controlling the adsorption process (Öztürk et al. 2020; Qi et al. 2020). While there are many ANN models in the literature, it can be said that the most widely used one, especially in engineering, is the multilayer model (Fan et al. 2018). ANN is beneficial when there is no mathematical relationship to describe a phenomenon to be modeled. ANN has reliable, robust, and remarkable features in finding nonlinear relationships of variables in complex systems. Due to these features, ANN is used in many applications. It is an essential model as it makes it possible to obtain more accessible and accurate numerical values at the stages where very complex and challenging modeling techniques are needed (Kwon et al. 2017). In this context, ANN draws much attention to modeling chemical and biochemical processes with complex input-output relationships (Chu 2003). In recent years, ANN models have been successfully applied in processes such as dye removal, adsorption, fermentation, filtration, and drying (Fan et al. 2018). In dye removal studies, ANN gives researchers essential clues using nonlinear regression data from the experimental system (Veeraragavan et al. 2021). In studies where ANN is applied to the adsorption system, the adsorption process is tried to be improved by choosing the %removal value as the estimation parameter (Erdem 2019). When the applications of ANN in the adsorption system were examined in the literature, Amouei et al. used sunflower seed powder as an adsorbent in Cd removal. In the study, they investigated pH, initial dyestuff concentration, and contact time and showed that the theoretical data obtained using the ANN approach were compatible with the experimental results (Amouei et al. 2013). Bingol et al. used ANN for copper removal with black cumin and determined the R^2 values as 0.89 and 0.93 for the training and test data sets, respectively (Bingöl et al. 2016). Garza-González et al., used 3 input data, 2 hidden layers, and 20 neurons in their study by examining methylene blue removal with the genetic algorithm ANN (Garza-González et al. 2011). Çoruh et al., investigated parameters such as waste adsorbent amount, initial dyestuff concentration, temperature, and contact time in batch system dyes removal. With the ANN approach, they defined three-layer, 4-neuron input data, 12-neuron hidden layer, and 1-neuron output data and found that the model they obtained was compatible with the system (Çoruh et al. 2014). Öztürk et al. 2020 investigated the adsorption of methylene blue in drinking water treatment plant waste sludge with ANN. They also stated that the system is well-modeled (Öztürk et al. 2020). The complex functional processes in the adsorption of environmental samples are predicted by modeling and simulating the adsorption process (Ghaedi and Vafaei 2017). The artificial intelligence technique, which is frequently preferred in the modeling of chemical and biochemical processes involving complex input-output relations, is a successful method in terms of obtaining easier and more accurate numerical values compared to very complex stages (Chu 2003; Kardam et al. 2013; Altintig, Balta, et al. 2022).

In the first stage of this study, the magnetic property of AC was gained by using the co-precipitation method. Physicochemical and morphological characterizations of the produced AC and the synthesized magnetic AC were performed using XRD, SEM/EDS, FT-IR, and BET analysis techniques. In the second stage, the developed magnetic AC was used in MB removal and the equilibrium data were evaluated with the adsorption isotherm model and thermodynamic equations. The third phase of the study aims to estimate the percentage removal and adsorption capacity in terms of multiple parameters using artificial intelligence based on real experimental results by establishing an ANN-based model. Then, using the experimental data obtained from the adsorption study of the magnetically coated activated carbon methylene blue dyestuff, the adsorption efficiency was estimated with the help of the ANN model. The adsorption study used a multi-layered structure as the ANN model. The ANN model data obtained with the data obtained from each adsorption experiment were evaluated by various statistical methods. The ANN model data obtained as a result of the study were compared with the experimental data.

Materials and methods

Chemicals

Pure water was used in all experimental studies. The chemicals, NaOH, HCl, Methylene Blue (MB)(M.F. $= C_{16}H_{18}ClN_3S_3.H_2O$, M.W. $= 319.86$ g/mol), ethanol, $FeSO_4 \cdot 7H_2O$, and $FeCl_3.6H_2O$ with analytic grade were purchased from Merck (Merck Co. Darmstadt, Germany). All chemicals used in the study are of analytical grade and no further purification process has been performed.

Preparation of magnetic activated carbon

AC/Fe_3O_4 obtained using the co-precipitation method was synthesized using a mixture of Fe^{3+} and Fe^{2+} and activated carbon. To synthesize AC/Fe_3O_4, 7.8 g $FeCl_3 \cdot 6H_2O$ was weighed, and 100 mL of deionized water was added to it. A few drops of concentrated $Fe(OH)_3$ were added to prevent precipitation, then fish were thrown into it and placed on a magnetic stirrer, and 3.9 g of it was added. It was heated by adding $FeSO_4 \cdot 7H_2O$. At 70 °C, 3.3 g of AC and 100 mL of 5 mol L^{-1} NaOH were added rapidly. After stirring for 120 min at 80 °C, this black mixture brought to room temperature was collected

with the help of a magnet. The obtained magnetic adsorbent was washed with distilled deionized water and filtered with blue band filter paper. After washing with distilled water and ethanol first, it was dried in an oven at 60 °C.

Characterization

The surface morphologies of the samples were carried out using JEOL-JSM-6060LV Scanning Electron Microscope (SEM). To take SEM images, the powdered samples were gold-plated to ensure conductivity. Surface functional groups were determined using SHIMADZU IR Prestige 21 brand Fourier transform infrared spectra (FTIR). The functional groups' molecular structure absorbance values were analyzed in the wavelength range of 400–4000 cm^{-1}. The crystal structure of the samples was determined using a RIGAKU D/Max2200 brand X-Ray diffractometer (XRD). Samples were analyzed in the range of 10–80° at points located between 2θ angles. Multi-point Brunauer–Emmett–Teller (BET) surface area (m^{2}g^{-1}), pore size (nm), micropore and Meso-macropore volumes (cm^{3}g^{-1}) using surface and pore characterization device (Micromeritics ASAP 2020) (S$_{BET}$) analysis was determined by the nitrogen (N$_2$) gas adsorption technique in a liquid nitrogen environment at 77 K. Before the BET analysis, the temperature in the degassing treatment applied to the sample was 300 °C and the time was 360 min.

Adsorption studies

Adsorption experiments were carried out in a batch bath system. An MB stock solution was prepared at 1000 mg L^{-1} concentration. Standard solutions (1–5 mg L^{-1}) and working solutions (50–500 mg L^{-1}) were prepared by diluting the stock solutions with deionized water (chemical resistance: 18 MΩ cm). 0.1 M NaOH or 0.1 M HCl solutions were used for the pH adjustment of MB solutions. After the adsorption process, the MB concentration in the solution was measured in 3 repetitions with a spectrophotometer (Shimadzu UV-Vis 1240) at the wavelength of 665 nm. In experimental studies, contact time (5–150 min), initial MB concentration (50–500 mg L^{-1}), adsorbent dose (0.05–0.5 g L^{-1}), initial pH values (2–9), temperature (298–318 K), contact time (5–180 min) the effects of parameters such as were measured and optimum values were determined. The MB adsorption efficiency of the AC/Fe$_3$O$_4$ composite was calculated by Equation (1):

$$q_e = \frac{(C_0 - C_e)V}{m} \tag{1}$$

where q_e (mg g^{-1}) is the adsorption capacity of MB, C$_0$ (mg L^{-1}) is the initial MB concentration, C$_e$ (mg L^{-1}) is the equilibrium concentration of adsorbate, V is the volume of solution (L) and m is the weight of adsorbent (g).

The paint removal percentage (MB) was calculated according to the following Equation (2):

$$Removal\ (\%) = \frac{(C_0 - C_e)}{C_0} \times 100 \tag{2}$$

Modeling of MB adsorption on AC/Fe$_3$O$_4$ with ANN

This study used the ANN approach for the dyestuff removal problem. The target is to estimate how much % of the dyestuffs in the wastewater are removed with specific parameters. The higher the %removal value, the better the removal results. This way, pollution in aquatic communities such as seawater, lake water, and streams will be prevented, and the negative impact on the ecosystem will be eliminated. For this purpose, initial solution pH, temperature, amount, contact time, and initial solution concentration parameters were used as input, %removal parameter, and adsorption capacity as an output parameter. Three distinct hidden input layers serve as the foundation for the ANN model, and the output layers, also known as neurons, are depicted in Figure 1. Inputs and outputs are used to estimate the relationship between layers.

Problem-solving was carried out using the MATLAB program and ANN method. The ANN model was compared using three different statistical criteria. These criteria are statistical parameters such as root mean square error (RMSE), mean absolute error (MAE), and correlation coefficient (R). In this study, 99% removal and 99 adsorption capacity data sets were taken, and 69 of them were used in training artificial neural networks, 15 in validation, and the remaining 15 testing ANNs. Normalized data at 0–1. For the data to be processed in the Matlab program, it is necessary to perform the normalization process. Therefore data (Xi) are converted to normalized value (X$_{normal}$) as follows (Rene et al. 2009).

$$X_{normal} = \frac{x_i - x_{\min}}{x_{\max} - x_{\min}} \tag{3}$$

In this equation; X_{normal} = stands for normalized data, x_i= for input value, x_{min}= for the least input value, and, $x_{\max}$= is used for the maximum input value.

The estimation process was carried out with 99 pieces of data. Levenberg–Marquardt Algorithm (LMA), a widely used neural network method, is generally used. The LMA algorithm contains multi-layer neural networks and has an input layer, hidden layers, and an output layer. There are many different types of training algorithms. ANNs are generally used to solve complex problems encountered in application areas such as model recognition, identification, classification, speech, vision, and control systems. It contains at least one or more layers, including an input layer, an output layer, and multiple hidden layers. There is no link between the units of the same layer; each neuron in a layer is connected to the neurons in the layer above and below it. Depending on the issue, the number of neurons in each layer may change (Arabameri et al. 2015)

Model validation

For the Validation of the Model, the following statistical indices such as mean squared error (MSE) are used to evaluate the integrity of the experimental data's fit and the model's predictive accuracy, respectively (Kalaivani and Ananthalakshmi 2018). MSE Equation (4) is presented
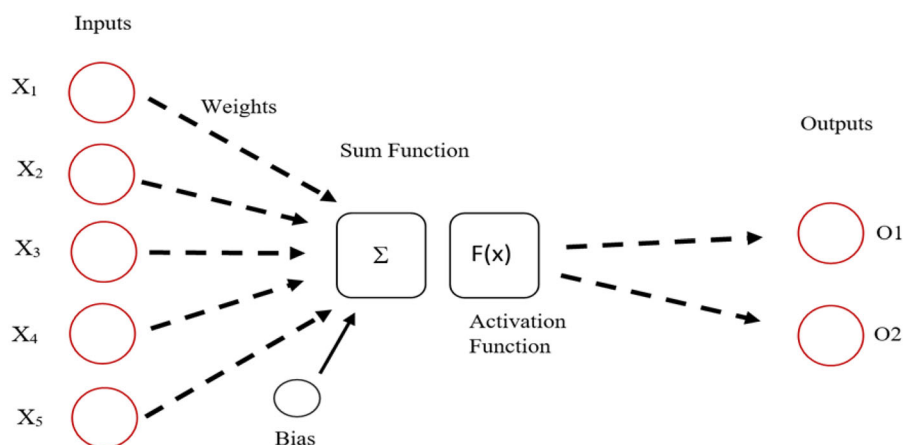
Figure 1. Schematic diagram of the ANN model.

below

$$MSE = \frac{1}{n}\sum_{t=1}^{n}(y_i - x_i)^2 \qquad (4)$$

The network was tested with different numbers of neurons to find the optimum number of neurons in the hidden layer by observing the *MSE*. The lowest *MSE* was shown for 6 neurons, and the maximum R^2 was obtained for 6 neurons. Table 7 shows the experimental situation for the neural network where pH, initial concentration, contact time, and dosage are input variables for the network. Table 8 displays the outcomes of a neural network's estimation (MSE and R^2) for training, validation, and testing.

Results and discussion

Characterization of AC/Fe₃O₄

Surface morphology of AC/Fe₃O₄ before and after adsorption SEM. To examine the surface morphology, the AC, and AC/Fe₃O₄ were subjected to SEM before and after the adsorption process. Figure 2a–c shows the SEM images (1000xmagnification).

Figure 2 shows SEM photographs of (a) AC (b) before MB adsorption AC/Fe₃O₄ and (c) AC/Fe₃O₄ after adsorption. Since AC has a porous structure when the SEM image is examined, it is thought that the cavities on the surface were previously filled by the chemical reagent, and these cavities on the surface of the activated carbon were formed by the evaporation of the activated carbon (Wang *et al.* 2005; Hadoun *et al.* 2013). When Fe₃O₄ loading occurs on AC, it is seen that the recesses and protrusions on the AC keep the particles on the surface. It is seen that MB adheres to the porous surface of AC/Fe₃O₄ and inside the crevices, while its surface has a more homogeneous appearance (c). As a result, adsorbents with small particle size, large surface area, and porous increased the adsorption capacity. Similar results have also been reported in the literature (Giri *et al.* 2011; Wannahari *et al.* 2018)

Figure 3 in (a–c), FT-IR spectra of activated carbon obtained from chestnut shells, AC/Fe₃O₄ samples before adsorption, and AC/Fe₃O₄ samples after adsorption is observed, respectively.

FT-IR analysis was performed to determine the structural groups of activated carbon, AC/Fe₃O₄ before adsorption, and AC/Fe₃O₄ samples after adsorption (Figure 3). The primary and secondary hydroxyl OH vibrations in Figure 3a show the overall spectral shape of AC exhibiting a bandwidth close to $3400\,cm^{-1}$ represented by y (–CH–OH) and y (–CH₂–OH) (Pandey, Son, Kim, *et al.* 2022). The peaks between 1000 and $1150\,cm^{-1}$ of activated carbon show the C–OH and C–O–H groups. The region between 1600 and $1800\,cm^{-1}$ is the specific region of pectin and is the region used in Deciphering pectin and determining its quality (Altintig *et al.* 2022). The peaks seen around $1750\,cm^{-1}$ are from olefinic C=C vibrations and C=O vibrations (Cao *et al.* 2014). While the peaks were sharp and prominent on the shell in activated carbon, the intensity of the OH-peak decreased, as can be seen in Figures 3b and c. Peaks between 500 and $600\,cm^{-1}$ in Figure 3b indicate metal-oxygen vibration. The sharpness of this peak decreased in Figure 3c. While the peaks were sharp and prominent on the shell in activated carbon, the intensity of the OH-peak decreased, as can be seen in Figure 3b and c. It is visible that there are changes in the functional groups of raw materials. There are similar studies in the literature (Mahmoodi 2013a; Jawad *et al.* 2022).

The XRD patterns of AC/Fe₃O₄ samples before and after AC and MB adsorption are shown in Figure 4.

XRD test was performed to determine whether the AC/Fe3O4 surface was crystalline or amorphous before and after AC adsorption. It is seen from the XRD patterns shown in Figure 4 that AC has an amorphous structure. However, after AC is converted to AC/Fe₃O₄, the amorphous nature of crude AC is minimized. Two broad peaks are observed in the AC XRD model at $2\theta = 25°$ and $2\theta = 43°$. Examining the X-ray diffraction profile of AC in Figure 4, the peaks shown at 25° and 43° confirm the carbonaceous structure in AC (Jawad *et al.* 2022). Figure 4 also shows the XRD results of AC/Fe₃O₄ and AC/Fe₃O₄/MB samples. Figure 4b, 30.3 (220) in the XRD spectrum; 35.5 (311); 43.3 (400); 54.1 (511); The characteristic peaks at 57.3 (511) and
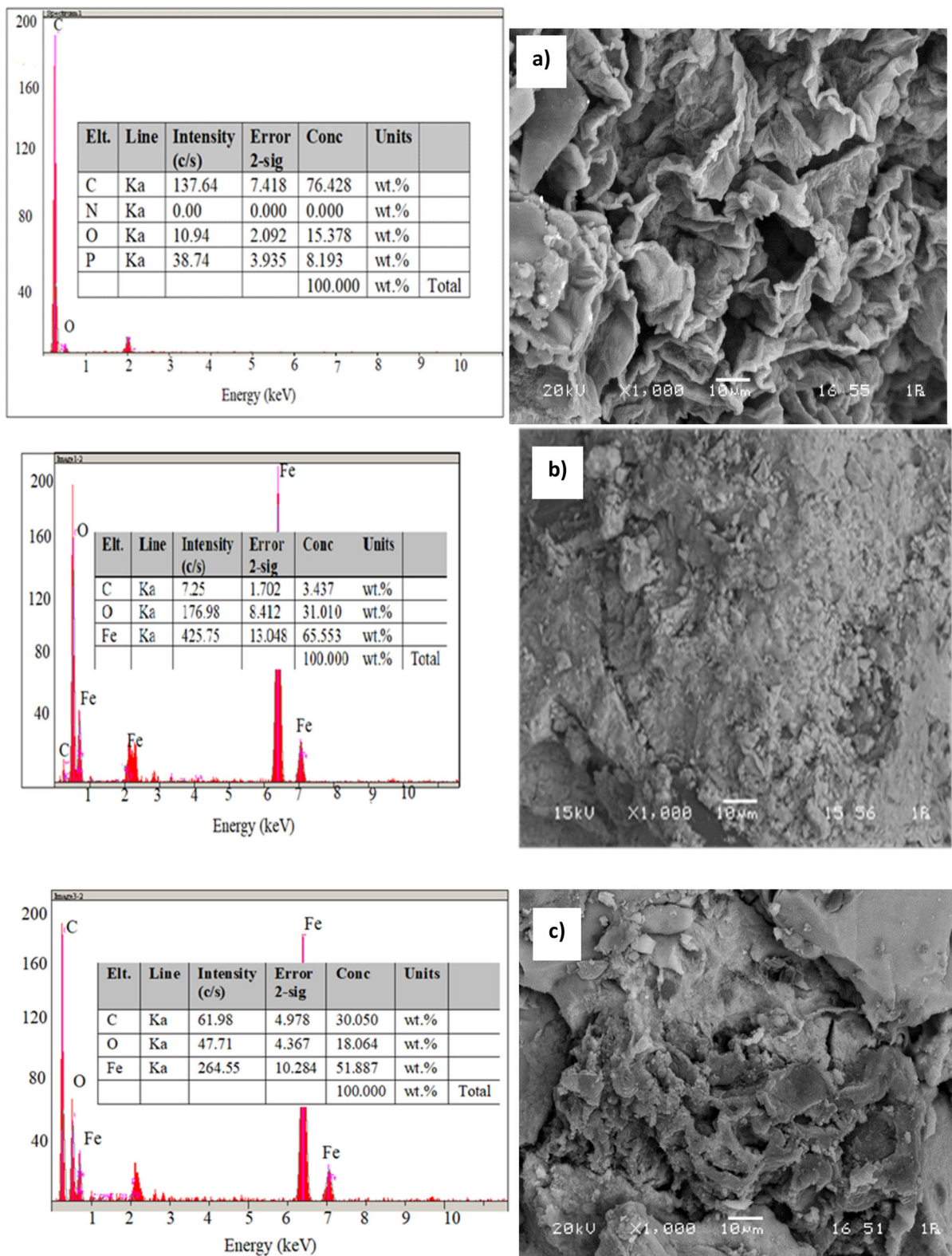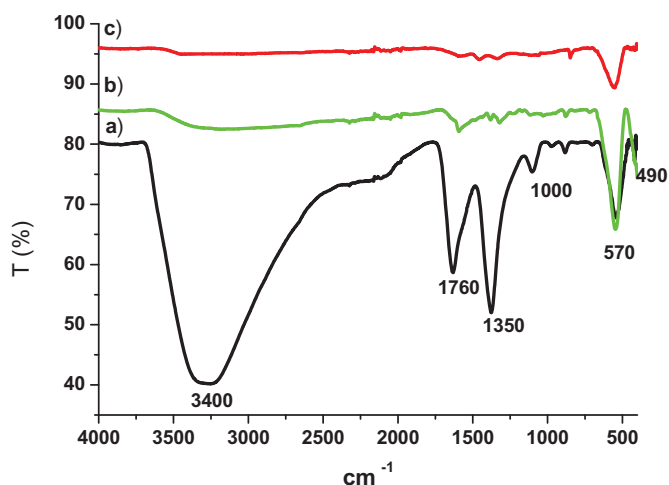
Figure 2. SEM results of (a) activated carbon (b) before MB adsorption AC/Fe₃O4 (c) after MB adsorption AC/Fe₃O₄.

62.9 (440) indicate that the magnetic AC is Fe₃O₄ (magnetite) and has a cubic spinel structure (Ai et al. 2011; Foroutan et al. 2019; Kheradmand et al. 2022). In Figure 4c, it is seen that the intensity of the peaks decreases after MB adsorption.

The surface treatment of adsorption and the extent of adsorption depend on the specific surface area. Adsorbents with small particle sizes, large surface areas, and porous structure increase adsorption (Díaz-Terán et al. 2003). Textural properties for AC and AC/Fe₃O₄ are given in Table 1.
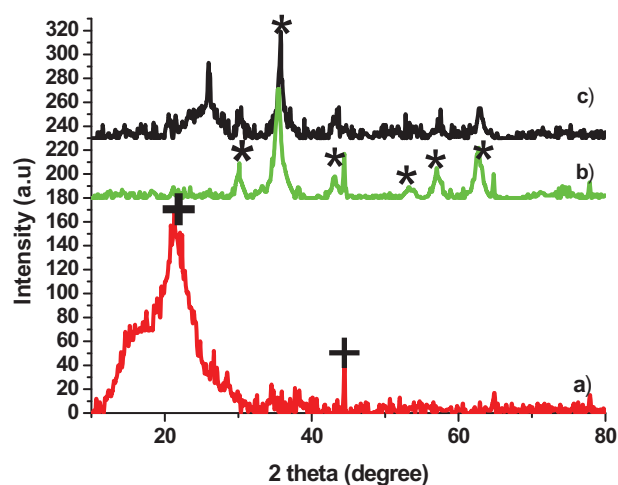
Figure 3. FTIR spectrum of (a) activated carbon (b) before MB adsorption AC/Fe₃O₄ (c)after MB adsorption AC/Fe₃O₄.

Figure 4. Powder XRD patterns, (a) activated carbon (b) before MB adsorption AC/Fe₃O₄ (c) after MB adsorption AC/Fe₃O₄.

In our study, BET surface area was $960.57\,m^2g^{-1}$ and micropore volume $0.26\,cm^3g^{-1}$ for AC, while it was $990.35\,m^2g^{-1}$ and $0.24\,cm^3$ for AC/Fe₃O₄ adsorbent, respectively. As can be seen in Table 1, the average pore diameter and surface area for iron oxide-coated AC/Fe₃O₄ are higher than for AC. In addition, as the micropores decreased, the pore diameter increased, but a more porous structure was obtained. Findings of mean pore diameter indicate the porous nature of AC and AC/Fe₃O₄ (2.0 nm < pore size range < 50 nm). This result explains that the increase in the pore diameter is due to the AC/Fe₃O₄ adsorption capacity.

Table 1. Textural properties of AC and AC/Fe₃O₄.

Adsorbents	S_{BET} ($m^2\,g^{-1}$)	Pore volume cm^3g^{-1}	Pore diameter (nm)
AC	960.57	0.26	20.07
AC/Fe₃O₄	990.35	0.24	22.31

Adsorption studies

pH is considered one of the most important factors affecting the surface charge density of the adsorbent and the diluted ion concentration in the solution. Thus, it implicitly affects the adsorption capacity (Pandey, Son, and Kang 2022). The influence of pH on MB adsorption on AC/Fe₃O₄ composite was studied with $0.1\,g\,L^{-1}$ dose at 298 K for $100\,mg\,L^{-1}$ dye concentrations. The dependency of the MB removal yield of AC/Fe₃O₄ on the pH of the solution is demonstrated in Figure 5a.

MB removal under acidic conditions is relatively lower (range of 66.36–92.6%) than under basic conditions. This difference may be due to the higher concentration of H^+ ions on the adsorbent surface and thus a reduction inMB retention (Jawad et al. 2018). Highest adsorption yields (92.65–99.82%) for initial concentrations were obtained at a pH value of 7. Therefore, pH 7.0 was chosen as the optimum pH value and used for all subsequent experiments. Similar results for MB removal have been reportedin the literature (Jawad et al. 2018; Jawad 2018). pHpzc is the change in pH values, pH end–pH start (ΔpH) when the pH is measured starting at zero. The point of zero charges (pHpzc) on the surface of AC/Fe₃O₄. was found to be 6.10 as illustrated in Figure 5b, signifying that the AC/Fe₃O₄ surface may gain a positive charge when pH is less than pHpzc. In turn, the surface charge of AC/Fe₃O₄ acquires negative charges at pH > pHpzc indicating that cationic MB dye can be adsorbed onto AC/Fe₃O₄. Considering the adsorption between the negatively charged surface and the cationic dyestuff, the excess H^+ ions in the environment at acidic pH values settle in sites suitable for adsorption on the AC/Fe₃O₄and prevent the adsorption of cationic dyestuffs. At a specific pH level, the surface charge of an adsorbent determines the type of interaction between the binding sites and the adsorbate molecules, and the zero charge point can accurately predicts the adsorption mechanism. In the case of cationic impurities, adsorption occurs if pH > pHpzc, conversely, adsorption of anionic impurities occurs if pH < pHpzc.

Adsorption kinetics

Adsorption kinetics is used to determine which mechanisms play a role during the adsorption of the adsorbed substance onto the adsorbent surface (Sharafi et al. 2015). Examining the kinetic curves provides data on AC/Fe₃O₄ stability, the decisive key step in the adsorption mechanism, and the time required to reach equilibrium (Jawad et al. 2022). Our study used pseudo-first- and pseudo-second-order models to understand the kinetics behind MB subtraction and to analyze kinetic data. The experiment was carried out in a 250 mL bottle by incorporating a mass of $0.1\,g\,L^{-1}$ of AC/Fe₃O₄ in 100 mL of the aqueous solution of MB with an initial concentration of 100 mg L^{-1}. The pH was adjusted to 7.0 with constant stirring of the sample at 500 rpm and room temperature ($25 \pm 2\,°C$). To determine the effect of contact time on adsorption, AC/Fe₃O₄ (0.1 g) samples were made with 100 mL MB $100\,mg\,L^{-1}$ solution. The samples were taken at defined time intervals, filtered with a 0.22 mm PTFE syringe filter, and then analyzed by spectrophotometer. The so-called first-order and pseudo-second-order equations are shown in equations 5 and 6 respectively.

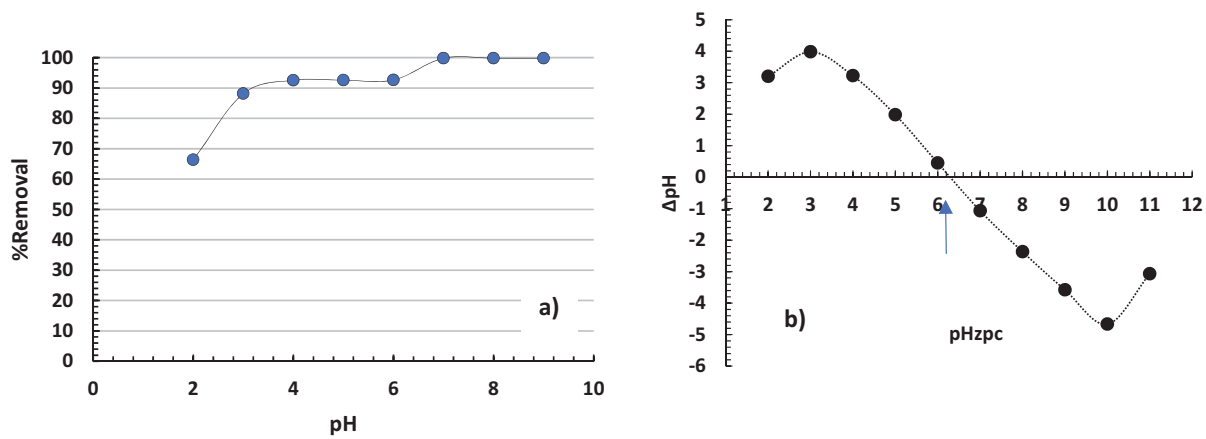$$ln\,(q_e - q_t) = \log q_e - \frac{k_1}{k_2}t \qquad (5)$$

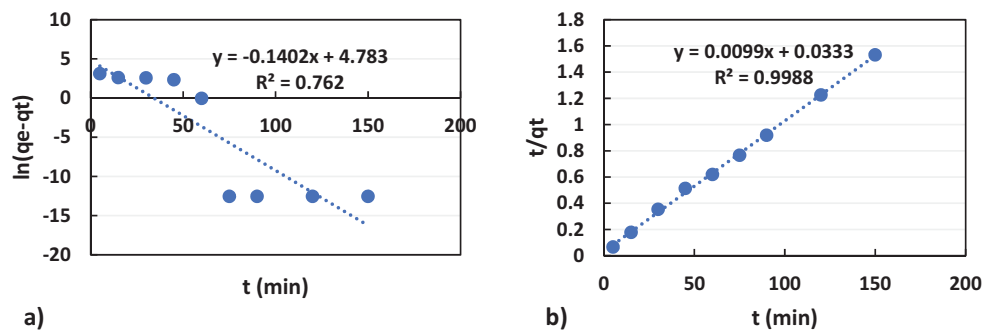**Figure 5.** (a) pH (b) PHpzc of AC/Fe$_3$O$_4$.

Figure 6. (a) Pseudo 1st order kinetic modeling results obtained for MB adsorption onto AC/Fe$_3$O$_4$ composite (b) Pseudo 2nd order kinetic modeling results obtained for MB adsorption onto AC/Fe$_3$O$_4$ composite (Initial MB concentration: 100 mg L^{-1}, adsorbent dose: 0.1 g L^{-1}, temperature: 298K).

$$\frac{t}{q_t} = \frac{1}{k_2 q_e^2} + \frac{t}{q_e} \qquad (6)$$

Here q_e and q_t are the amounts of adsorbed material (mg g^{-1}) at equilibrium time (min), respectively; k_1 (h^{-1}) is the first-order kinetic constant, and k_2 is that of the pseudo-second-order kinetics (g mg^{-1}).

Pseudo-first-order and Pseudo second order profiles (Figures 6a and b) and kinetic properties (Table 2) are shown. It reflects that the adsorption of MB dye on AC/Fe$_3$O$_4$ fits the Pseudo first-order model because the R^2 value calculated from the Pseudo second-order was higher than the other applied model. Moreover, the experimental q_e values agreed satisfactorily with the calculated $q_e cal$ values obtained.

Pseudo 1 and pseudo 2 results of AC/Fe$_3$O$_4$ were given in Table 2. The adsorption capacity (q_{eexp}) value propounded experimentally in Table 2 under ideal conditions should be close to the calculated adsorption capacity (q_{ecal}) value. In Table 2, the adsorption process does not comply with the velocity requirements of pseudo 1st order due to the difference between q_{eexp} and q_{ecal}, and the correlation coefficient value not being close to 1 (Shayesteh et al. 2021; Jawad et al. 2022). On the other hand, a very high correlation coefficient was achieved by the pseudo 2nd order kinetic model.

Adsorption thermodynamics

In the thermodynamic study, changes in Gibbs free energy ($\Delta G°$), enthalpy ($\Delta H°$), and entropy ($\Delta S°$) parameters were calculated using Equations (7)–(9). In addition, the $\Delta G°$ parameter is calculated by considering the equilibrium time distribution constant (KL).

$$\Delta G^o = -RT ln\ KD \qquad (7)$$

In the equation, R is the gas constant (8.314 J mol^{-1}K^{-1}), T is the temperature, and K_L is the thermodynamic equilibrium constant reflecting the dye distribution in the equilibrium between solid and liquid phases. The equilibrium constant (K_D) is calculated as in equation 8.

$$KL = \frac{qe}{Ce} \qquad (8)$$

The van't Hoff equation is given in 9.

$$ln\ K_L = \frac{\Delta S^o}{R} - \frac{\Delta H^o}{RT} \qquad (9)$$

The values of $\Delta H°$(kj mol^{-1}) and $\Delta S°$ (J/mol K) were calculated from the intersection and slope of the van't Hoff plots ln KD versus 1/T, (Jawad et al. 2018; Jawad et al. 2020) as shown in Figure 7. The parameters calculated through the values of thermodynamics Figure 7 are presented in Table 3.

Table 3 shows the computed thermodynamic parameters. Table 3 shows that the negative values of $\Delta G°$ were

belonging to the MB dye adsorption by AC/Fe$_3$O$_4$ in the temperature ranges (298–318) K.

As seen from Table 3, the positive value of $\Delta S°$ indicates increased randomness at the solid/liquid interface of the adsorption process of MB. The calculated negative values of $\Delta G°$ indicate that the adsorption of MB on the AC/Fe$_3$O$_4$ system is spontaneous and thermodynamically favorable. In the MB adsorption study performed with AC/Fe$_3$O$_4$, the $\Delta H°$ value was found to be 20.40 kj mol^{-1}. In this case, it is thought that the adsorption mechanism using AC/Fe$_3$O$_4$ may be chemical. Similar results for methylene blue dye adsorption have been reported in the literature (Jawad et al. 2018; Yousef et al. 2022).

Adsorption isotherm models

Adsorption isotherms are used to investigate the interactions between adsorbents and adsorbates and the distribution of solutes between solid and liquid phases (Mahmoodi 2014c). The reaction mechanism of the adsorption system can be deduced by some theoretical or empirical models. Langmuir and Freundlich'isotherms are widely used to study the relationship between adsorption capacity and the equilibrium concentration of adsorbate at a given temperature. In this study, using 0.1 g L^{-1} AC/Fe$_3$O$_4$ activated carbon and 100 mL of different initial MB concentrations (50–500 mg L^{-1}), isotherms should be used by demonstrating the relationship between the equilibrium concentrations reached and the amount of adsorbed substance per unit adsorbate. Modeling was done using Langmuir and Freundlich isotherm model to show the relationship between MB amounts per adsorbent unit (Abdulhameed et al. 2022). The linear formula of this model is presented in (10).

$$\frac{C_e}{q_e} = \frac{1}{q_m K_L} + \frac{1}{q_m} Ce \qquad (10)$$

C_e is the adsorbate concentration in the solution after adsorption (mg L^{-1}), q_e is the amount adsorbed on the adsorbent (mg g^{-1}), KL is the isotherm coefficient (L mg^{-1}), q_{max} (mg g^{-1}) is the maximum adsorption capacity of the adsorbent.

The Freundlich isotherm model assumes that the adsorbent surface is multilayered by adsorbent molecules. This linear formula is presented in Equation (11).

$$ln q_e = ln K_f + \frac{1}{n} C_e \qquad (11)$$

In the formula, K_f and n stand for Freundlich constants. Modeling was done using Langmuir and Freundlich isotherm model to show the relationship between MB amounts per adsorbent unit. These models are shown in Figures 8 and b.

In this study, using 0.1 g L^{-1}AC/Fe$_3$O$_4$ activated carbon and 100 mL different initial MB concentrations (50–500 mg L^{-1}), isotherms should be used by revealing the relationship between the equilibrium concentrations reached and the amount of adsorbed substance per unit adsorbent. Modeling was done using Langmuir and Freundlich isotherm model to show the relationship between MB amounts per adsorbent unit. The Langmuir and Freundlich isotherm constant obtained by the calculations is presented in Table 4 as follows.

As can be seen in Table 4, the maximum adsorption capacity of AC/Fe$_3$O$_4$ was calculated according to the slope and intersection points of the q_{max} graphs and was calculated as 277.77 mg g^{-1}. Considering the experimental data obtained, it can be said that the correlation coefficient (R^2) value of 0.99 is compatible with the Langmuir isotherm.

A value of $1/n < 1$ indicates strong adsorption bonding as a result of strong intermolecular attraction within the adsorbent layers. A value of n between 2 and 10 indicates good adsorption. However, in this case, when the value falls between 1 and 2, it indicates medium adsorption capacity, and n value less than 1 indicates undesired adsorption capacity (Jawad et al. 2018). In our study, the $1/n$ value was calculated as 0.47. The $n = 2.10$ value obtained from this study indicates beneficial adsorption. According to the results of Table 4, it is clear that MB has the potential to be an effective and economical adsorbent for removal of water.

Reusability study

Both anionic and cationic dyes can be removed from aqueous solutions using adsorbent materials. However, the use of such materials may be limited due to some environmental concerns due to the tdisposal of the adsorbent

$y = -2469.8x + 12.201$
$R^2 = 0.9835$
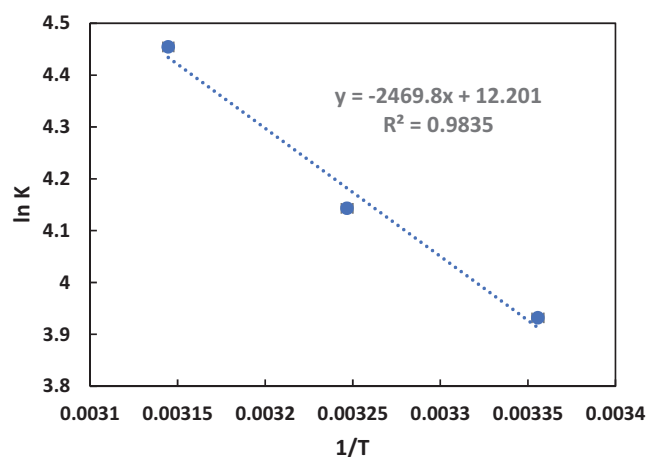
Figure 7. Van't Hoff plot for MB dye adsorption onto AC/Fe$_3$O$_4$ (adsorbent dose 0.1 g L^{-1}, pH of 7 volume of solution 100 mL, and agitation speed 250 rpm).

Table 2. Kinetic results determined based on pseudo 1st and 2nd-order kinetic models.

Pseudo 1st order				Pseudo 2nd order		
$q_{e\ exp}$ k_1, min^{-1}	q_{ecal}(mg g^{-1})	R^2	k_2 (g.mg^{-1}.min^{-1})	q_{ecal} (mg g^{-1})	R^2
97.96 0.1402	119.46	0.76	0.03	101.01	0.99

Table 3. Thermodynamic parameters for MB dye adsorption onto AC/Fe$_3$O$_4$.

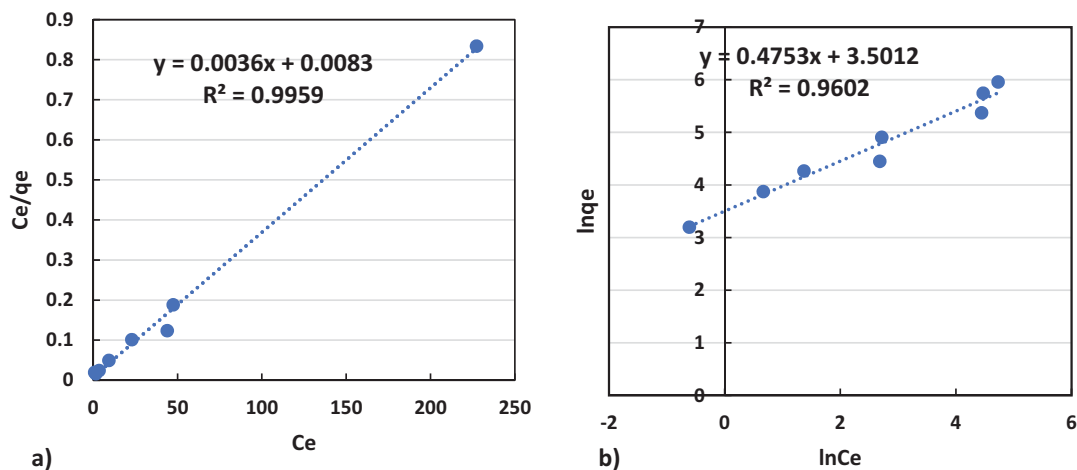| Sample	T (K)	$\Delta G°$ (kJ mol^{-1})	$\Delta S°$ (kJ mol^{-1} K^{-1})	$\Delta H°$ (kJ mol^{-1})
AC/Fe$_3$O$_4$	298	−9.74	0.101	20.40
	308	−10.60		
	318	−11.77		

Figure 8. (a) AC/Fe$_3$O$_4$ activated carbon Langmuir (b) Freundlic isotherms.

Table 4. Langmuir and Freundlich isotherms equation parameters.

Sample	q_m(mg/g)	b(l/mg)	R^2	K_f	n(l/mg)	R^2
AC/Fe$_3$O$_4$	277.77	0.43	0.996	33.15	2.10	0.961

after saturation. Desorbing dye molecules and regenerating adsorbents are alternative approaches for the disposal of spent adsorbents (Alakhras *et al.* 2022). MB desorption efficiency was investigated using four different concentrated eluents: 0.1 M NaOH, 0.2 M NaOH, 0.1 M HCl, and 0.2 HCl. Desorption efficiency was determined as being 73.42, 78.7, 89.16, and 98.56%, respectively. As can be seen from these results, the maximum desorption efficiency was achieved by using 0.2 M HCI solution and, was therefore was selected as the optimum eluent. Reusability performance is one of the important criteria for cleaning processes. For the 0.2 M HCl eluent, the adsorption-desorption process was followed and checked. Considering this important feature, an eight-cycle adsorption/desorption process was performed to determine the reusable performance of the Fe$_3$O$_4$/AC adsorbent for the removal of MB from the aquatic environment. The reusability yield (%) for each cycle is shown in Figure 9.

Only about a 15% reduction in adsorption efficiency occurred during the first four cycles, and although the desorption efficiency was almost constant, it reached about 27% after the 8th cycle. The decrease in the capacity of the adsorbent we produced may be due to the partial deactivation of the adsorption sites during the cycling process. As a result, it is clearly seen that the developed Fe$_3$O$_4$/AC adsorbent exhibits a favorable reuse performance during the removal of MB from the aqueous medium.

It is also shown that it is suitable for the adsorption and removal of MB from aqueous solutions. Table 5 shows the comparison of MB adsorption capacities with different adsorbents in the literature.

Proposal of the possible adsorption mechanisms

The binding of MB dye to AC/Fe$_3$O$_4$ was mainly investigated from the results of pHpzc studies, and the possible adsorption mechanism is graphically illustrated in Figure 10. The possible adsorption mechanism of MB cationic dye on AC/Fe$_3$O$_4$ can occur in 3 ways: (1) electrostatic attraction, (2) hydrogen bonding and (3) pi–pi interactions.

Performance graph

The data set was used to determine the optimal architecture of the ANN model, the maximum R^2 value and minimum MSE value of the test. The training process was carried out using the standard backpropagation algorithm as the optimization procedure. Figure 11 shows the error performance graph of the training and test sets obtained from the experimental results.

Figure 11 shows how the error values of the training and test data at each step changed as a result of the training. The best performance value indicates the point at which the minimum error is reached. As seen in the graph, the training of the network reached an optimum result in the 12th step.

Comparison of actual value and estimated values

Figure 12 (a) comparison of actual and estimated %removal values, (b) compares graphics of actual and estimated adsorption capacities are shown.

In comparison to the normalized data collected from the experiment, Figures 12a and b show the estimated values of the normalized removal data for the training and test datasets using the ANN model. As can be seen from Figure13, the actual and estimated values are quite close to each other. Chowdhury and Saha, in their study in 2013, defined the optimal topology for MB removal using the 3-13-1 process with R^2 0.9951. (Chowdhury and Saha 2013). As a result, it was determined that the predicted results of the ANN model we applied and the experimental results were in harmony and that the developed ANN model represented the experiments. Figure 13 shows the histogram graph of the experimental data we used in our study.

When the histogram graph in Figure 13 is examined, it shows a normal distribution which supports the use of linear regression. Based on this idea, our experimental data set was
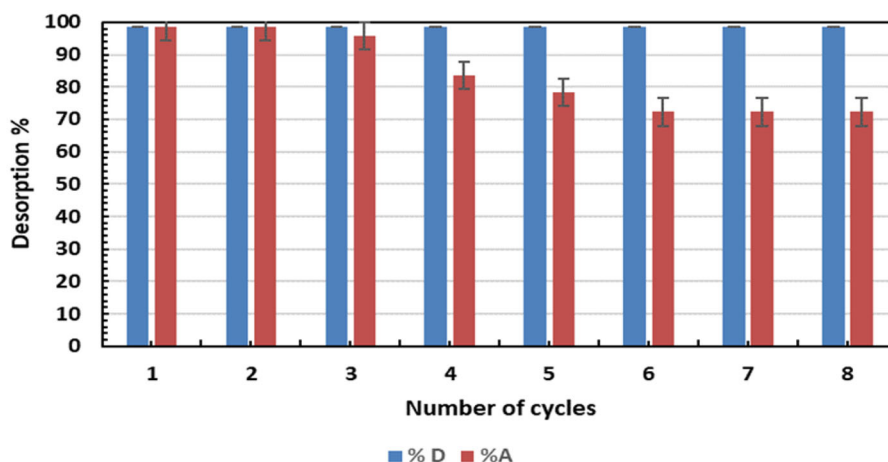
Figure 9. Reusability yield (%) for eight adsorption/desorption cycles (298 K, adsorbent dose: 0.10 g 0.1 L^{-1}, pH: 7).

Table 5. Comparison of MB adsorption capacity of different kinds of adsorbents reported in the literature.

| Adsorbent	q_{max} (mg /g)	Isotherm	Adsorption kinetic	Ref.
Microalgae	297.1	Langmuir	Pseudo-second order	Abdulhameed et al. 2022
Mangosteen peels activated carbon (MSPAC)	163.6	Langmuir	Pseudo-second order	Jawad et al. 2022
Watermelon peel (WMP)	312.8	Langmuir	Pseudo- second order	–
Activated carbon (MSMPAC)	232.8	Langmuir	Pseudo-second order	Razali et al. 2022
Pumice powder	35.71	Langmuir	Pseudo second order	Sharafi et al. 2015
Pomelo fruit peel	218.5	Langmuir	Pseudo-second order	Dinh et al. 2019
AC/Fe$_3$O$_4$	277.77	Langmuir	Pseudo-second order	This study
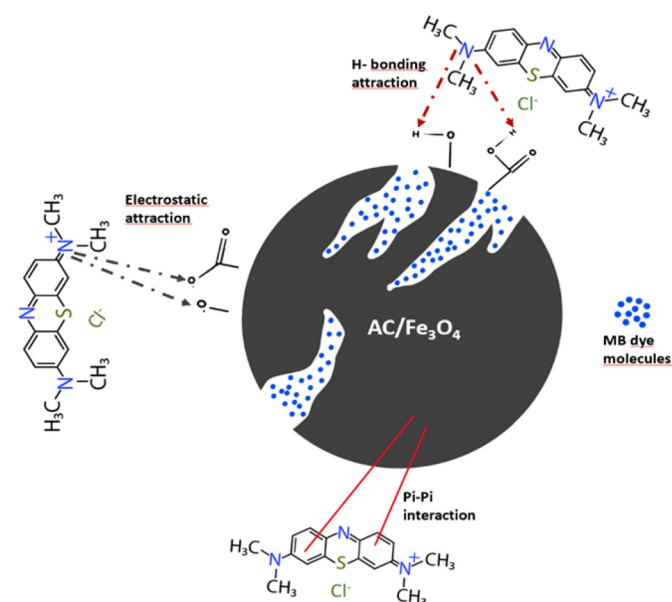
Figure 10. The possible mechanism between the dyestuff and the adsorbent.

analyzed using multiple linear regression, since the independent variable used was more than one.

Modeling of dye adsorption with artificial neural networks approach

In the study, which was carried out by changing the number of neurons in the hidden layer for dye adsorption, it was determined that the best ANN model was a network with 10 neurons. ANN modeling graph is shown in Figure 14.

As can be seen in Figure 14, the ANN model successfully predicted the optimal structure from the training data (a).

Although there is significant data scatter, it also performed reasonably well during testing and validation (Figures 8b and c). According to Figure 14, the ANN model performed well overall for the batch adsorption experimental dataset (d). In the ANN model shown in Figure 14, with the help of the mean square error (MSE), a value of 13.20127e^{-0} for the training data is obtained for the validation dataset, but 0.9983 for the training data, 0.9939 for the validation dataset, and 0.9939 for the test dataset. There are similar findings in studies in the literature.

In this study, % removal and adsorption capacity were performed with the use of ANN and regression analysis in dyestuff removal. The Mean Absolute Percent Error (MAPE) method statistically evaluated experimental and estimation values. Equation (12) was used to calculate the error with MATLAB Outputs.

$$\text{MAPE} = 100 * \frac{\sum_{i=1}^{n} \left| \frac{Real_i - Estimated}{Real_i} \right|}{n} \qquad (12)$$

MAPE = 0.0248   0.0845 is displayed as.

Plotting experimental and prognostic data yields the R-value utilized in ANN investigations. On the other hand, the R^2 value is a statistical technique used to assess the degree of linearity between two variables or the link between a variable and two or more other variables. In our investigation, the neuron in the hidden layer was chosen, and it was selected based on the R^2 value achieved through a method of trial and error.

Normality assumption

The normal distribution of the data is important for multiple linear regression analysis. In this study, normality analysis was performed in the SPSS program and the results are given Table 6.
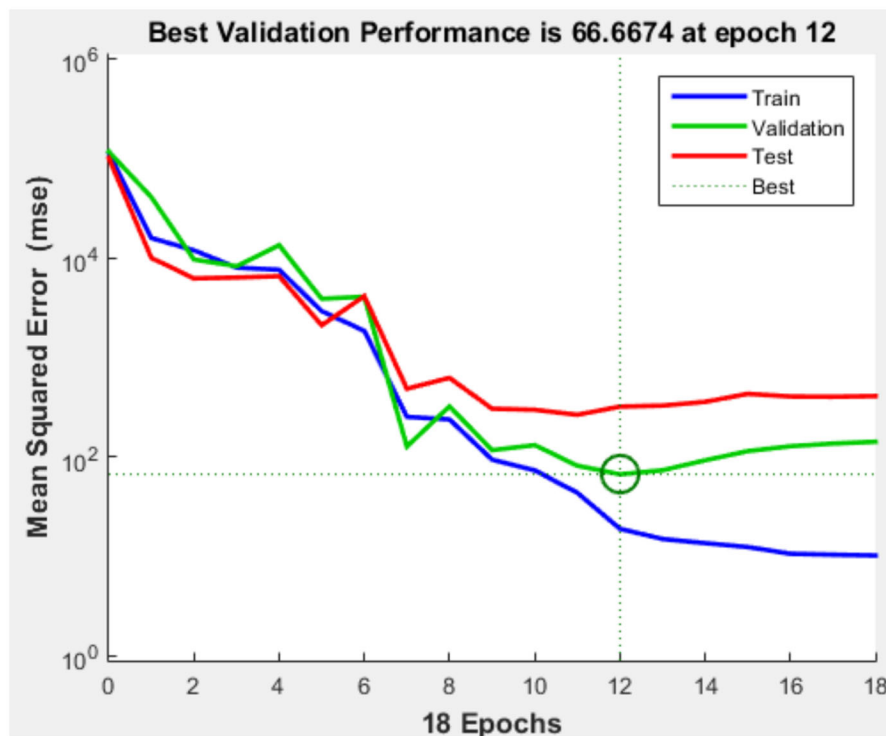
Figure 11. Error performance graph for training and test data.
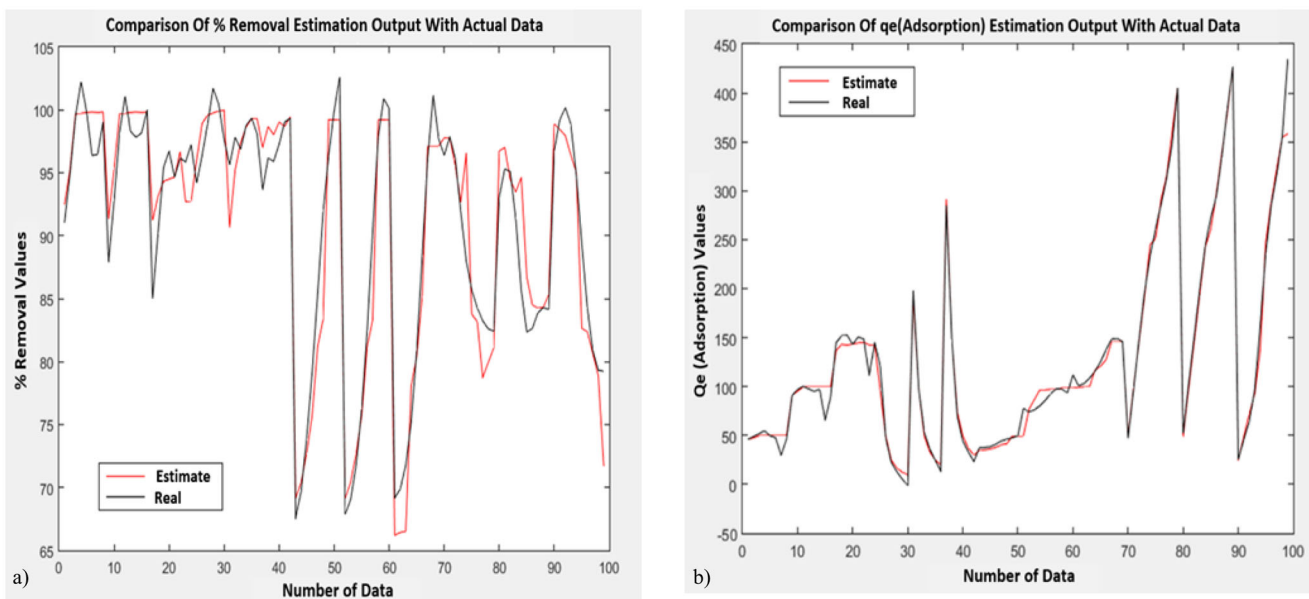
Figure 12. (a) Comparison of percent removal estimation output with actual output, (b) comparison of q_e (adsorption capacity) estimated output with actual output.

The hypotheses are set up as follows:

H0: data are normally distributed with 95% confidence.
H1: data are not normally distributed with 95% confidence.

As seen in Table 6, "Kolmogorov–Smirnov" and "Shapira–Wilk" tests were applied in the analysis of normality. All H_0 hypotheses were accepted since the "Sig" values were greater than 0.05. The data are normally distributed at the 95% confidence interval. In this context, the p value was accepted as 5%. The p value is usually "Sig." in packaged programs, expressed by abbreviation. "Sig." "significance is the abbreviation of the word "significance.

Normality analysis can also be checked by looking at the Skewness and Kurtosis values. If these values are between -1.5 and $+1.5$, it is assumed that they are normally distributed. (Jani *et al.* 2022) Since the values marked in Table 7 are between -1.5 and $+1.5$, it has been proven that the data used complies with the normality assumption.
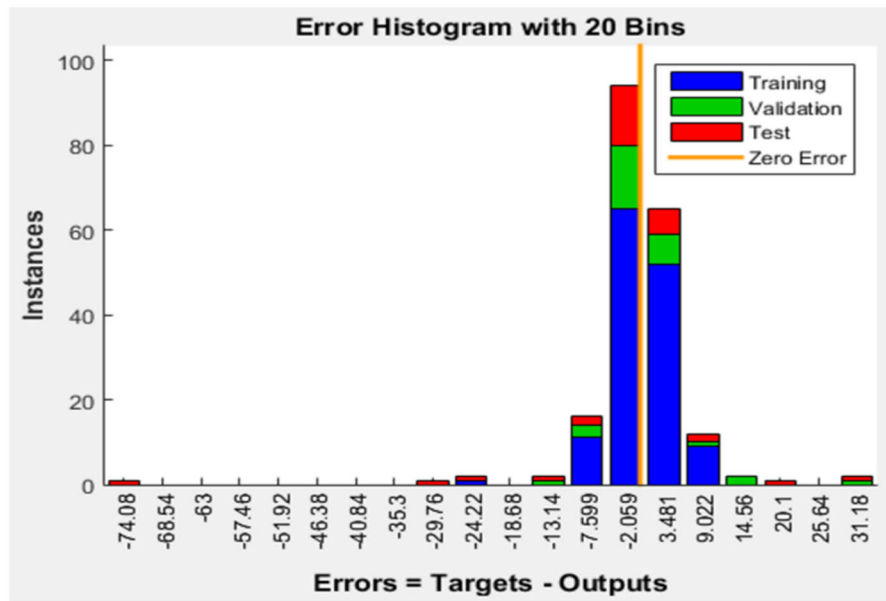
Figure 13. Histogram graph.
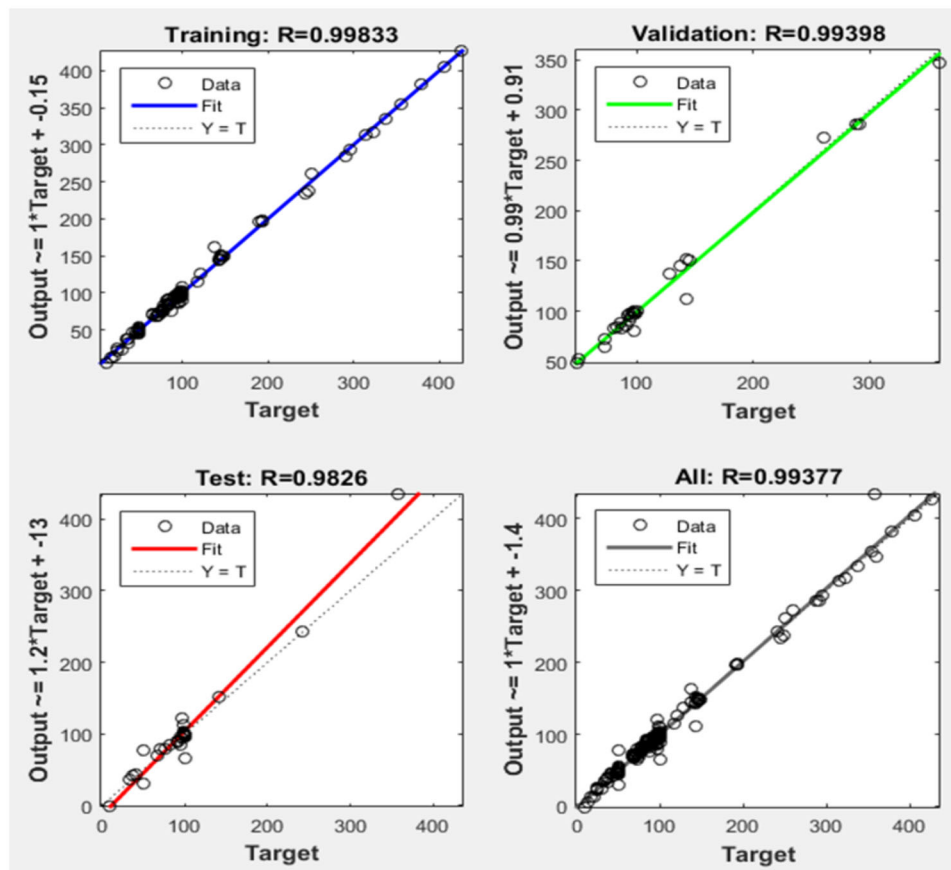
Figure 14. ANN modeling graph.

Figure 15a shows the % removal Normality Test Graph and Figure 15b shows the Adsorption Capacity) Normality Test Graph.

Looking at the graphs in Figure 14a and b, it is seen that the data is in line with the curve. This shows that the data fit the normality distribution graphically.

Regression and statistics tests

Regression and statistical tests were performed in SPSS and their outputs are given in Table 8) below.

a. Dependent variable:%Removal
b. All requested variables entered.

Since the most used method is the "Enter" method, this method was used in the selection of variables. The feature of the "Enter" method is that it simultaneously includes the arguments in the system. As an output, the effect of each independent variable on the model was evaluated. A model summary of % removal and q_e (Adsorption capacity) is given in Table 9.

Tables 9 give the % removal and q_e (Adsorption capacity) summaries of the models. When these summaries are examined, the R^2 value for the % reduction was found to be 0.801. However, since the model fits multiple regression, the adjusted R^2 value should be taken into account. It is seen that this value is 0.790. Therefore, the effect of 5 independent variables on the dependent variable is 80%. The remaining 20% are other parameters that are not included in the system. For q_e (Adsorption capacity), the R^2 value was found to be 0.944. However, since the model fits multiple regression, the adjusted R^2 value should be taken into account. It is seen that this value is 0.941. Therefore, the effect of 5 independent variables on the dependent variable is 94%. The remaining 6% are other parameters that are not included in the system. As can be seen from Table 9 the values of adjusted R^2 is lower than R^2, which reflects the good quality of the model. Similar results are seen in the literatüre (Jaafari et al. 2020).

In Table 10, the % removal coefficients and significance values for the regression model are given, and in Table 10, the q_e (Adsorption Capacity) coefficients and significance values are given.

Table 10 show the coefficients and significance values for the regression model. The coefficient of the constant term was calculated as 67.221 q_e (Adsorption Capacity) 57.913 for %removal and its value was specified as less than 0.001 for

%removal. 0.002 was found for q_e Since both are less than 0.05, they have a 5% significance level. It was concluded that the variables were significant.

ANOVA test results for % removal and q_e are given in Table 11.

The F test results in Table 11 are for use for y our model. It is therefore not intended for the F test.

Although artificial intelligence and ANN studies are close to real experimental results, they are also very important in terms of sustainability. It is an indicator of sustainability, as it is environmentally and cost-effective. In our study, the fact that the results of real experiments are approximate to the results of ANN experiments shows that this study is appropriate in terms of feasibility analysis.

Table 6. Test of normality.

	Kolmogorow-Smirnov[a]			Shapiro-Wilk		
	Sitatistic	df	Sig.	Sitatistic	df	Sig.
%Removal	0.212	99	0.073	0.824	99	0.164
q_e	0.214	99	0.074	0.844	99	0.164

[a]Predictors (Concentration, temperature, time, pH, dosage).

Table 7. Kurtosis and skewness values.

|			Statistic	Std. error
		Descriptives		
%Removal	Mean		90.842	1.006
	95%Confidence interval for mean Lower bound		88.846	
	Upper bound		92.840	
	5% Trimmed mean		91.640	
	Median		95.285	
	Variance		100.250	
	Std. deviation		10.012	
	Minimum		66.190	
	Maximum		99.952	
	Range		33.762	
	Interquartile range		15.821	
	Skewness		−1.020	0.243
	Kurtosis		−0.196	0.481
q_e	Mean		127.553	10.139
	95%Confidence interval for mean Lower bound		107.433	
	Upper bound		147.673	
	5% Trimmed mean		119.350	
	Median		98.495	
	Variance		10.176	
	Std. deviation		100.878	
	Minimum		9.995	
	Maximum		426.647	
	Range		416.652	
	Interquartile range		96.125	
	Skewness		1.282	0.243
	Kurtosis		0.821	0.481
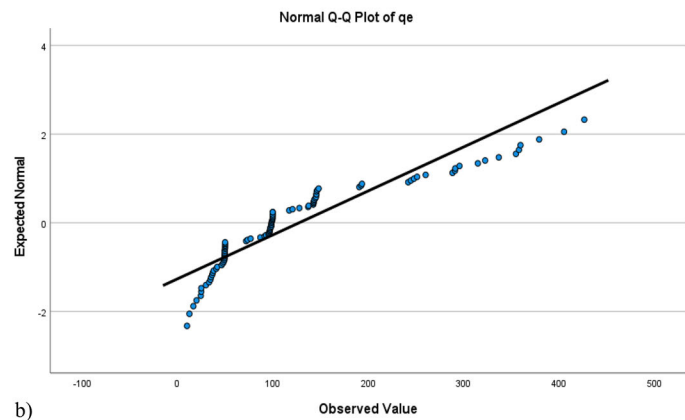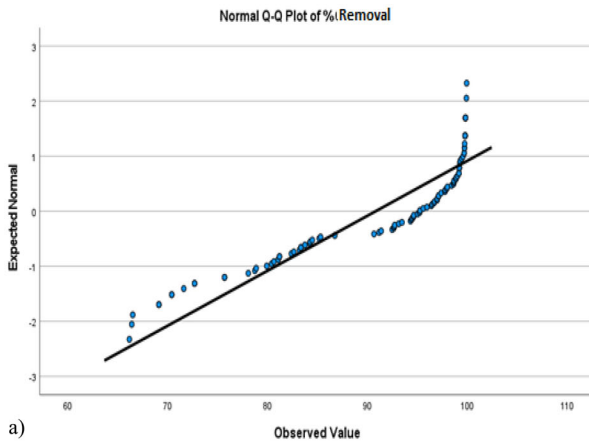
Figure 15. (a) %Reduction Normality Test Graph, (b) q_e (adsorption capacity) Normality Test Graph.

Table 8. Input data for %removal and q_e.

		Variables entered/Removed		
	Model	Variables entered	Variables removed	Method
%Removal	1	Temperature, time, pH, adsorbent dosage, concentration[a]		Enter
q_e	1	Temperature, time, pH, adsorbent dosage, concentration[b]		Enter

[a]Dependent Variable: %Removal.
[b]Dependent Variable q_e.

Table 9. Model summary.

	Model	R	R square	Adjusted R square	Std. The error in the estimate	R square change	F change	df1	df2	Sig. F change
%Removal	1	0.895[a]	0.801	0.790	4.585985415	0.801	74.827	5	93	<.001
q_e	1	0.972[a]	0.944	0.941	24.45371117	0.944	314.950	5	93	<.001

[a]Predictors (Concentration, temperature, time, pH, dosage).

Table 10. % Removal and q_e coefficients and significance values.

		Coefficients				
		Unstandardized coefficients		Standardized coefficients		
	Model	B	Std.Error	Beta	t	Sig
	1(Constant)	67.221	3.388		19.842	<.001
	pH	−0.049	0.364	−0.006	−0.134	0.033
%Removal	Time	0.300	0.013	0.788	16.681	<0.001
	Concentration	−0.39	0.005	−0.462	−8.624	<0.001
	Dosage	17.013	5.192	0.156	3.277	0.001
	Temperature	0.098	0.083	0.063	1.180	0.241
	1(Constant)	57.913	18.064		3.206	0.002
q_e	pH	1.083	1.939	0.014	0.559	0.048
	Time	0.286	0.096	0.075	2.989	0.004
	Concentration	0.815	0.024	0.0956	33.746	<0.001
	Dosage	−256.061	27.686	−0.233	−9.249	<0.001
	Temperature	1.894	0.444	−0.121	−4.269	<0.001

Table 11. %Removal and ANOVA.

		ANOVA				
	Model	Sum of squares	df	Mean square	F	Sig.
	1 Regression	7.868	5	1.573711	74.827	<.001[a]
%Removal	Residual	1.955464	93	21.031		
	Total	9.824464	98			
	1 Regression	941.676499	5	188.3353	74.827	<.001[b]
q_e	Residual	55.612511	93	597.984		
	Total	997.289010	98			

[a]Dependent Variable:%Removal.
[b]Dependent Variable q_e. Predictors: (Constant), temperature, time, pH, dosage, concentration.

Conclusion

An AC/Fe$_3$O$_4$ adsorbent has been effectively employed to remove MB cationic dye from aqueous solutions. SEM/EDS, FTIR, and XRD results showed that the composite was successfully prepared. Adsorption experiments showed that the pseudo-second-order model provided the best description of the kinetic uptake properties, while the adsorption results at equilibrium were explained by the Langmuir model, where the maximum adsorption capacity (q_{max}) was 277.7 mg g^{-1}. Thermodynamic parameters show that the adsorption process is endothermic in nature and is a spontaneous adsorption process. The % removal rate and adsorption were estimated using the simplest possible architecture built on the ANN architecture and taking into account the values of the other variables at a time "t" and the values before this time at a certain time "t". The Levenberg–Marquardt algorithm was used, and the number of neurons was determined as 10. The results found that the predictive values were 2% and 8%, respectively, and the R^2 value was 99%. For the training, validation, and test datasets, it was seen that the R^2 values were very close to 1, the MSE values were very small, and the output data predicted by the models was in harmony with the experimental data. These ANN models represent the adsorption of dyestuffs. In addition, the results of the F tests are shown for the whole model. Therefore, when the F test values were examined, it was concluded that the model is completely statistically significant. As a final result, the regression model and statistical tests were found to be significant. The results showed that neural network modeling could effectively predict MB removal from AC/Fe$_3$O$_4$. In future studies, modeling studies for the removal of other water pollutant categories such as heavy metals, pesticides, herbicides and antibiotics can be investigated with the AC/Fe$_3$O$_4$ adsorbent.

Ethical approval

Our article was not sent to more than one journal for simultaneous evaluation. No data, texts, or theories of others are presented in our article. We do not have any data belonging to any person whose publication permission.

Author contributions

Zeynep Aydemir contributed to the design and execution of the experiments and calculation of the data, while Dilay Bozdag and Eren Kılıç contributed to artificial intelligence and statistical calculations. Assoc. Dr. Esra Altıntığ contributed to the experiments' visualization, interpretation, supervision, and arrangement. Assoc. Dr. Tijen Over Ozcelik and Assoc. Dr. Ayten Yılmaz Yalçıner artificial intelligence and statistical comments contributed to the editing.

Disclosure statement

No potential conflict of interest was reported by the author(s).

Funding

Data availability statement

We do not have any person's data in any form. Consent for publication is Not applicable.

References

Abdulhameed AS, Jawad AH, Kashi E, Radzun KA, ALOthman ZA, Wilson LD. 2022. Insight into adsorption mechanism, modeling, and desirability function of crystal violet andmethylene blue dyes by microalgae: Box-Behnken design application. Algal Res. 67:102864.

Abdurrahman FB, Akter M, Abedin Z. 2013. Dyes removal from textile wastewater usingorange peels. Int J Sci Technol Res. 2(9):47–50.

Agarwal S, Tyagi I, Gupta VK, Bagheri AR, Ghaedi M, Asfaram A, Hajati S, Bazrafshan AA. 2016. Rapid adsorption of ternary dye pollutants onto copper(I) oxide nanoparticle loaded on AC: experimental optimization via response surface methodology. J Chem Eng. 4(2):1769–1779. doi:10.1016/j.jece.2016.03.002.

Ahmad R, Aslam M, Park E, Chang S, Kwon D, Kim J. 2018. Submerged low-cost pyrophyllite ceramic membrane filtration combined with GAC as fluidized particles for industrial wastewater treatment. Chemosphere. 206:784–792. doi:10.1016/j.chemosphere.2018.05.045.

Ahmadi S, Mohammadi L, Rahdar A, Rahdar S, Dehghani R, Igwegbe CA, Kyzas GZ. 2020. Acid dye removal from aqueous solution by using neodymium(III) oxide nanoadsorbents. Nanomaterials. 10(3):556. doi:10.3390/nano10030556.

Ai L, Zhang C, Liao F, Wang Y, Li M, Meng L, Jiang J. 2011. Removal of methylene blue from aqueous solution with magnetite loaded multi-wall carbon nanotube: kinetic, isotherm, and mechanism analysis. J Hazard Mater. 198:282–290. doi:10.1016/j.jhazmat.2011.10.041.

Alakhras F, Ouachtak H, Alhajri E, Rehman R, Al-Mazaideh G, Anastopoulos I, Lima EC. 2022. Adsorptive removal of cationic rhodamine B dye from aqueous solutions using chitosan-derived Schiff base. Sep Sci Technol. 57(4):542–554. doi:10.1080/01496395.2021.1931326.

Altintig E, Balta S, Balta M, Aydemir Z. 2022. Methylene blue removal with ZnO coated montmorillonite: thermodynamic, kinetic, isotherm and artificial intelligence studies. Int J Phytoremediation. 24(8):867–880. doi:10.1080/15226514.2021.1984386.

Altintig E, Kabadayi O, Bozdag D, Altundag S, Altundag H. 2022. Artificial neural network mathematical modeling of methyl violet removal with chitosan-coated clinoptilolite. DWT. 250:252–265. doi:10.5004/dwt.2022.28247.

Altintig E, Yenigun M, Sarı A, Altundag H, Tuzen M, Saleh TA. 2021. Facile synthesis of zinc oxide nanoparticles loaded activated carbon as an eco-friendly adsorbent for ultra-removal of malachite green from water. Environ Technol Innov 21:101305.

Amouei A, Amooey AA, Asgharzadeh F. 2013. A study of cadmium removal from aqueous solutions by sunflower powders and its modeling using artificial neural network. Iran J Health Sci. 1(3):28–34.

Angın D. 2014. Production and characterization of activated carbon from sour cherry stones by zinc chloride. Fuel. 115:804–811.

Arabameri M, Javid A, Roudbari A. 2015. The use of artificial neural network (ANN) for modeling ammonia nitrogen removal from landfill leachate by the ultrasonic process. Int J Health Studies. 1(3):13–19.

Balarak D, Jaafari J, Hassani G, Mahdavi Y, Tyagi I, Agarwal S, Gupta VK. 2015. The use of low-cost adsorbent (Canola residues) for the adsorption of methylene blue from aqueous solution: ısotherm, kinetic and thermodynamic studies. Colloids Interface Sci Commun. 7:6–19.

Bianco L, D'Amico E, Villone A, Nanna F, Barisano D. 2020. Bioremediation of wastewater stream from syngas cleaning via wet scrubbing. Chem Eng Trans. 80:31–36.

Bingöl D, Kılıç E, Hercan M. 2016. Bakır biyosorpsiyon işlemine Yapay Sinir Ağı (ANN) yaklaşımı. Sakarya University J Sci. 20(3):433–440. doi:10.16984/saufenbilder.25723.

Boguniewicz-Zablocka J, Klosok-Bazan I, Callegari A, Capodaglio AG. 2020. Snack-food industry effluent pre-treatment for annatto dye and yeast removal: process improvement for effectiveness and sustainability. J Clean Prod. 277:124117. doi:10.1016/j.jclepro.2020.124117.

Cao C, Xiao L, Chen C, Shi X, Cao Q, Gao L. 2014. In situ preparation of magnetic Fe_3O_4/chitosan nanoparticles via a novel reduction-precipitation method and their application in adsorption of reactive azo dye. Powder Technol. 260:90–97. doi:10.1016/j.powtec.2014.03.025.

Chowdhury S, Saha PD. 2013. Artificial neural network (ANN) modeling of adsorption of methylene blue by NaOH-modified rice husk in a fixed-bed column system. Environ Sci Pollut Res Int. 20(2):1050–1058. doi:10.1007/s11356-012-0912-2.

Chu KH. 2003. Prediction of two-metal biosorption equilibria using a neural network. Eur J Miner Process Environ Prot. 3(1):119–127.

Çoruh S, Kılıç E, Geyikci F. 2014. Prediction of adsorption efficiency for the removal of malachite green and acid blue 161 dyes by waste marble dust using ANN. Glob Nest J. 16(4):676–689.

D'Cruz B, Madkour M, Amin MO, Al-Hetlani E. 2020. Efficient and recoverable magnetic AC-Fe_3O_4 nanocomposite for rapid removal of promazine from wastewater. Mater Chem Phys. 240:122109. doi:10.1016/j.matchemphys.2019.122109.

Dehghani MH, Mahdavi P. 2015. Removal of acid 4092 dye from aqueous solution by zinc oxide nanoparticles and ultraviolet irradiation. Desal Water Treat. 54(12):3464–3469. doi:10.1080/19443994.2014.913267.

Díaz-Terán J, Nevskaia DM, Fierro JLG, López-Peinado AJ, Jerez A. 2003. Study of chemical activation process of lignocellulosic material with KOH by XPS and XRD. Microporous Mesoporous Mater. 60(1–3):173–181. doi:10.1016/S1387-1811(03)00338-X.

Dibi K, Meite L, Aboua KN, Soro DB, Konan G, Kossonou NR, Traore SK, Mamadou K. 2021. Optimizing the preparation conditions of activated carbon from coconut shells using a full factorial design optimizing the preparation conditions of activated carbon from coconut shells using a full factorial design. IJIAS. 33:214–221.

Dinh V, Huynh TDT, Le HM, Nguyen V, Dao V, Hung NQ, Tuyen LA, Lee S, Yi J, Duy T, Nguyen, Tan LV. 2019. Insight into the adsorption mechanisms of methylene blue and chromium(III) from aqueous solution onto pomelo fruit peel. RSC Adv. 9:25847.

Erdem F. 2019. S. cerevisiae ile Remozal Sarı (RR) Giderimine Yapay Sinir Ağı (YSA) Yaklaşımı. Uludağ Üniversitesi Mühendislik Fakültesi Dergisi. 24(2):289–297.

Fan MY, Hu JW, Cao RS, Ruan WQ, Wei XH. 2018. A review on experimental design for pollutant removal in water treatment with the aid of artificial intelligence. Chemosphere. 200:330–343. doi:10.1016/j.chemosphere.2018.02.111.

Fernandes CD, Nascimento VRS, Meneses DB, Vilar DS, Torres NH, Leite MS, Vega Baudrit JR, Bilal M, Iqbal HMN, Bharagava RN, et al. 2020. Fungal biosynthesis of lignin-modifying enzymes from pulp wash and Luffa cylindrica for azo dye RB5 biodecolorization using modeling by response surface methodology and artificial neural network. J Hazard Mater. 399:123094. doi:10.1016/j.jhazmat.2020.123094.

Foroutan R, Mohammadi R, Razeghi J, Ramavandi B. 2019. Performance of algal activated carbon/Fe_3O_4 magnetic composite for cationic dyes removal from aqueous solutions. Algal Research. 40:101509. doi:10.1016/j.algal.2019.101509.

Garza-González MT, Alcalá-Rodríguez MM, Pérez-Elizond R, Cerino-Córdova FJ, Garcia-Reyes RB, Loredo-Medrano JA, Soto-Regalado E. 2011. Artificial neural network for predicting biosorption of methylene blue by Spirulina sp. Water Sci Technol. 63(5):977–983. doi:10.2166/wst.2011.279.

Ghaedi AM, Vafaei A. 2017. Applications of artificial neural networks for adsorption removal of dyes from aqueous solution: a review. Adv Colloid Interface Sci. 245:20–39. doi:10.1016/j.cis.2017.04.015.

Gharanjig K, Arami M, Bahrami H, Movassagh B, Mahmoodi NM, Rouhani S. 2008. Synthesis, spectral properties, and application of novel monoazo disperse dyes derived from N-ester-1,8-naphthalimide to polyester. Dyes Pigm. 76(3):684–689. doi:10.1016/j.dyepig.2007.01.024.

Giri SK, Das NN, Pradhan GC. 2011. Synthesis and characterization of magnetite nanoparticles using waste iron ore tailings for adsorptive removal of dyes from aqueous solution. Colloid Surf Physicochem Eng Asp. 389(1–3):43–49. doi:10.1016/j.colsurfa.2011.08.052.

Hadoun H, Sadaoui Z, Souami N, Sahel D, Toumert I. 2013. Characterization of mesoporous carbon prepared from date stems by H₃PO₄ chemical activation. Appl Surf Sci. 280:1–7. doi:10.1016/j.apsusc.2013.04.054.

Hamd A, Dryaz AR, Shaban M, AlMohamadi H, Abu Al-Ola KA, Soliman NK, Ahmed SA. 2021. Fabrication and application of zeolite/acanthophora spicifera nanoporous composite for adsorption of Congo Red dye from wastewater. Nanomaterials. 11(9):2441–2461. doi:10.3390/nano11092441.

Hussain MS, Rehman R, Imran M, Dar A, Akram M, Al-Abbad EA. 2022. Eco-friendly detoxification of Congo Red dye from water by citric acid activated bioadsorbents consisting of watermelon and water chestnuts peels collected from ındigenous resources. Adsorp Sci Technol. doi:10.1155/2022/9056288.

Hynes NRJ, Kumar JS, Kamyab H, Sujana JAJ, Al-Khashman OA, Kuslu Y, Ene A, Suresh Kumar B. 2020. Modern enabling techniques and adsorbents based dye removal with sustainability concerns in textile industrial sector-a comprehensive review. J Clean Prod. 272:122636. doi:10.1016/j.jclepro.2020.122636.

Jaafari J, Barzanouni H, Mazloomi S, Farahani NAA, Sharafi K, Soleimani P, Haghighat GA. 2020. Effective adsorptive removal of reactive dyes by magnetic chitosan nanoparticles: kinetic, isothermal studies and response surface methodology. Int J Biol Macromol. 164:344–355. doi:10.1016/j.ijbiomac.2020.07.042.

Jani NA, Haddad L, Abdulhameed AS, Jawad AH, ALOthman ZA, Yaseen ZM. 2022. Modeling and optimization of the adsorptive removal of crystal violet dye by durian (*Durio zibethinus*) seeds powder: insight into kinetic, isotherm, thermodynamic, and adsorption mechanism. Biomass Conv Bioref. doi:10.1007/s13399-022-03319-x.

Jawad AH. 2018. Carbonization of rubber (*Hevea brasiliensis*) seed shell by one-step liquid phase activation with H₂SO₄ for methylene blue adsorption. DWT. 129:279–288. doi:10.5004/dwt.2018.23090.

Jawad AH, Abdulhameed AS, Reghioua A, Yaseen ZM. 2020. Zwitterion composite chitosan-epichlorohydrin/zeolite for adsorption of methylene blue and reactive red 120 dyes. Int J Biol Macromol. 163:756–765. doi:10.1016/j.ijbiomac.2020.07.014.

Jawad AH, Abdulhameed AS, Wilson LD, Syed-Hassan SSA, ALOthman ZA, Khan MR. 2021b. High surface area and mesoporous activated carbon from KOH-activated dragon fruit peels for methylene blue dye adsorption: optimization and mechanism study. Chin J Chem Eng. 32:281–290. doi:10.1016/j.cjche.2020.09.070.

Jawad AH, Mallah SH, Mastuli MS. 2018. Adsorption behavior of methylene blue on acid-treated rubber (*Hevea brasiliensis*) leaf. DWT. 124:297–307. doi:10.5004/dwt.2018.22915.

Jawad AH, Saber SEM, Abdulhameed AS, Reghioua A, ALOthman ZA, Wilson LD. 2022. Mesoporous activated carbon from mangosteen (*Garcinia mangostana*) peels by H₃PO₄ assisted microwave: optimization, characterization, and adsorption mechanism for methylene blue dye removal. Diam Relat Mater. 129:109389. doi:10.1016/j.diamond.2022.109389.

Joseph J, Radhakrishnan RJ, Johnson JK, Joy SP, Thomas J. 2020. Ion-exchange mediated removal of cationic dye-stuffs from water using ammonium phosphomolybdate. Mat Chem Phy. 242:1–8.

Kalaivani S, Ananthalakshmi S. 2018. ANN Modeling and GA Optimization of zinc removal from wash water by electro-coagulation process. Int J Future Rev Computer Sci Commun Eng. 4(3):393–399.

Kant S, Pathania D, Sing P, Dhiman P, Kumar A. 2014. Removal of malachite green and metylene blue by Fe0.01Ni0.01Zn0.98O/polyacrylamide nanocomposite using coupled adsorption and photocatalysis. Appl Catal B. 147:340–352. doi:10.1016/j.apcatb.2013.09.001.

Karami A, Karimyan K, Davoodi R, Karimaei M, Sharafie K, Rahimi S, Khosravi T, Miri M, Sharafi H, Azari A. 2017. Application of response surface methodology for statistical analysis, modeling, and optimization of malachite green removal from aqueous solutions by manganese-modified pumice adsorbent. DWT. 89:150–161. doi:10.5004/dwt.2017.21366.

Kardam A, Raj KR, Arora JK, Srivastava S. 2013. Simulation and optimization of artificial neural network modeling for prediction of sorption efficiency of nanocellulose fibers for removal of Cd (II) ions from aqueous system. Eng Phys Sci. 11(6):497–508. doi:10.2004/wjst.v11i6.625.

Katheresan V, Kansedo J, Lau SY. 2018. Efficiency of various recent wastewater dye removal methods: a review. J Environ Chem Eng. 6(4):4676–4697. doi:10.1016/j.jece.2018.06.060.

Khedr SA, Shouman MA, Attia AA. 2013. Adsorption studies on the removal of cationic dye from shrimp shell using chitin. Biointerface Res Appl Chem. 3(1):507–519.

Kheradmand A, Negarestani M, Mollahosseini A, Shayesteh H, Farimaniraad H. 2022. Low-cost treated lignocellulosic biomass waste supported with FeCl₃/Zn(NO₃)₂ for water decolorization. Sci Rep. 12(1):16442. doi:10.1038/s41598-022-20883-4.

Kwon SK, Jung HS, Baek WK, Kim D. 2017. Classification of forest vertical structure in south Korea from aerial orthophoto and lidar data using an artificial neural network. Appl Sci. 7(10):1046–1059. doi:10.3390/app7101046.

Mahmoodi NM. 2013a. Synthesis of amine-functionalized magnetic ferrite nanoparticle and ıts dye removal ability. J Environ Eng. 139(11):1382–1390. doi:10.1061/(ASCE)EE.1943-7870.0000763.

Mahmoodi NM. 2013b. Photodegradation of dyes using multiwalled carbon nanotube and ferrous ıon. J Environ Eng. 139(11):1368–1374. doi:10.1061/(ASCE)EE.1943-7870.0000762.

Mahmoodi NM. 2014a. Dendrimer functionalized nanoarchitecture: synthesis and binary system dye removal. J Taiwan Inst Chem Eng. 45(4):2008–2020. doi:10.1016/j.jtice.2013.12.010.

Mahmoodi NM. 2014b. Binary catalyst system dye degradation using photocatalysis. Fibers Polym. 15(2):273–280. doi:10.1007/s12221-014-0273-1.

Mahmoodi NM. 2014. Synthesis of core–shell magnetic adsorbent nanoparticle and selectivity analysis for binary system dye removal. J Ind Eng Chem. 20(4):2050–2058. doi:10.1016/j.jiec.2013.09.030.

Mahmoodi NM. 2015. Surface modification of magnetic nanoparticle and dye removal from ternary systems. J Ind Eng Chem. 27:251–259. doi:10.1016/j.jiec.2014.12.042.

Mahmoodi MN, Arami M. 2009. Numerical finite volume modeling of dye decolorization using immobilized titania nanophotocatalysis. Chem Eng J. 146(2):189–193. doi:10.1016/j.cej.2008.05.036.

Mahmoodi MN, Arami M, Limaee NY, Gharanjig K, Ardejani FD. 2006. Decolorization and mineralization of textile dyes at solution bulk by heterogeneous nanophotocatalysis using immobilized nanoparticles of titanium dioxide. Colloid Surf A-Physicochem Eng Asp. 290(1–3):125–131. doi:10.1016/j.colsurfa.2006.05.012.

Mahmoodi NM, Arami M, Limaee NY, Gharanjig K, Nourmohammadian F. 2007. Nanophotocatalysis using immobilized titanium dioxide nanoparticle degradation and mineralization of water containing organic pollutant: case study of Butachlor. Mater Res Bull. 42(5):797–806. doi:10.1016/j.materresbull.2006.08.031.

Mahmoodi NM, Limaee NY, Arami M, Borhany S, Taheri MM. 2007. Nanophotocatalysis using nanoparticles of titania mineralization and finite element modelling of solophenyl dye decolorization. J Photochem Photobiol A. 189(1):1–6. doi:10.1016/j.jphotochem.2006.12.025.

Mahmoodi NM, Shourijeh ZM. 2015. Preparation of PVA-chitosan blend nanofiber and ıts dye removal ability from colored wastewater. Fibers Polym. 16(9):1861–1869. doi:10.1007/s12221-015-5371-1.

Mahmoodi MN, Arabloo M, Abdi J. 2014. Laccase immobilized manganese ferrite nanoparticle: synthesis and LSSVM intelligent modeling of decolorization. Water Res. 67:216–226. doi:10.1016/j.watres.2014.09.011.

Mahmoodi MN, Arami M, Limaee NY, Gharanjig K, Ardejani FD. 2006. Decolorization and mineralization of textile dyes at solution bulk by heterogeneous nanophotocatalysis using immobilized

nanoparticles of titanium dioxide. Colloid Surf A-Physicochem Eng Asp. 290:125–131.

Mokhtari HA, Bagheri M, Mirbagheri SA, Akbari A. 2020. Performance evaluation and modeling of an integrated municipal wastewater treatment system using neural networks. Water Environ J. 34(S1):622–634. doi:10.1111/wej.12565.

Oladoye PO, Ajiboye TO, Omotola EO, Oyewola OJ. 2022. Methylene blue dye: toxicity and potential elimination technology from waste-water. Results Eng. 16:100678. doi:10.1016/j.rineng.2022.100678.

Öztürk N, Senturk HB, Gündoğdu A, Duran C. 2020. Drinking water treatment plant with methylene blue adsorption on waste slud and modeling with artificial neural networks. Uludağ Uni J Faculty Eng. 25(2):1083–1104.

Pandey S, Makhado E, Kim S, Kang M. 2023. Recent developments of polysaccharide based superabsorbent nanocomposite for organic dye contamination removal from wastewater—a review. Environ Res. 217:114909. doi:10.1016/j.envres.2022.114909.

Pandey S, Son N, Kang M. 2022. Synergistic sorption performance of karaya gum crosslink poly (acrylamide-co-acrylonitrile) @ metal nanoparticle for organic pollutants. Int J Biol Macromol. 210:300–314. doi:10.1016/j.ijbiomac.2022.05.019.

Pandey S, Son N, Kim S, Balakrishnan D, Kang M. 2022. Locust Bean gum-based hydrogels embedded magnetic iron oxide nanoparticles nanocomposite: advanced materials for environmental and energy applications. Environ Res. 214(Pt 3):114000. doi:10.1016/j.envres.2022.114000.

Qi J, Hou Y, Hu J, Ruan W, Xiang Y, Wei X. 2020. Decontamination of Methylene Blue from simulated wastewater by the mesoporous rGO/Fe/Co nanohybrids: artificial intelligence modeling and optimization. Mater Today Commun. 24:100709. doi:10.1016/j.mtcomm.2019.100709.

Qu W, Yuan T, Yin G, Xu S, Zhang Q, Su H. 2019. Effect of 488 properties of activated carbon on 489 malachite green adsorption. Fuel. 249:45–53. doi:10.1016/j.fuel.2019.03.058.

Rahdar S, Rahdar A, Sattari M, Hafshejani LD, Tolkou AK, Kyzas GZ. 2021. Barium/Cobalt@polyethylene glycol nanocomposites for dye removal from aqueous solutions. Polymer. 13(7):1161. doi:10.3390/polym13071161.

Rahdar S, Rahdar A, Zafar MN, Shafqat SS, Ahmad S. 2019. Synthesis and characterization of MgO supported Fe–Co–Mn nanoparticles with exceptionally high adsorption capacity for Rhodamine B dye. J Mater Res Technol. 8(5):3800–3810. doi:10.1016/j.jmrt.2019.06.041.

Rajkumar D, Song BJ, Kim JG. 2007. Electrochemical degradation of reactive blue 9 in chloride medium for the treatment of textile dyeing wastewater with identification of intermediate compounds. Dyes Pigm. 72(1):1–7. doi:10.1016/j.dyepig.2005.07.015.

Razali NS, Abdulhameed AS, Jawad AH, ALOthman ZA, Yousef TA, Al-Duaij OK, Alsaiari NS. 2022. High-surface-area-activated carbon derived from mango peels and seeds wastes via microwave-ınduced ZnCl₂ activation for adsorption of methylene blue dye molecules: statistical optimization and mechanism. Molecules. 27(20):6947. doi:10.3390/molecules27206947.

Rehman R, Anwar J, Mahmud T. 2012. Thermodynamical and ısothermal modeling of methylene blue dye batch biosorption on formalin modified Madhuca longifolia leaf powder. J Chem Soc Pak. 34(2):460–467.

Rene ER, Veiga MC, Kennes C. 2009. Experimental and neural model analysis of styrene removal from polluted air in a biofilter. J Chem Technol Biotechnol. 84(7):941–948. doi:10.1002/jctb.2130.

Saleh TA, Tuzen M, Sarı, A, Naeemullah . 2017. Polyethylenimine modified activated carbon as novel magnetic adsorbent for the removal of uranium from aqueous solution. Chem Eng Res Des. 117:218–227., doi:10.1016/j.cherd.2016.10.030.

Sen TK, Afroze S, Ang HM. 2011. Equilibrium, kinetics and mechanism of removal of methylene blue from aqueous solution by adsorption onto pine cone biomass of pinus radiata. Water Air Soil Pollut. 218(1–4):499–515. doi:10.1007/s11270-010-0663-y.

Shamey R, Zhao X. 2014. Modelling, simulation and control of the dyeing process. Amsterdam: Elsevier.

Sharafi K, Mansouri AM, Zinatizadeh AA, Pirsaheb M. 2015. Adsorptive removal of methylene blue from aqueous sılutions by pumice powder: process modelling and kinetic evaluation. Environ Eng Manag J. 14(5):1067–1078. doi:10.30638/eemj.2015.118.

Sharafi K, Pirsaheb M, Gupta VK, Agarwal S, Moradi M, Vasseghian Y, Dragoi E-N. 2019. Phenol adsorption on scoria stone as adsorbent – application of response surface method and artificial neural networks. J Mol Liq. 274:699–714. doi:10.1016/j.molliq.2018.11.006.

Shayesteh H, Kelishami AR, Norouzbeigi R. 2016. Evaluation of natural and cationic surfactant modified pumice for congo red removal in batch mode: kinetic, equilibrium, and thermodynamic studies. J Mol Liq. 221:1–11. doi:10.1016/j.molliq.2016.05.053.

Shayesteh H, Raji F, Kelishami AR. 2021. Influence of the alkyl chain length of surfactant on adsorption process: a case study. Surf Interfaces. 22:100806. doi:10.1016/j.surfin.2020.100806.

Suhaimi A, Abdulhameed AS, Jawad AH, Yousef TA, Duaij KA, ALOthman ZA, Wilson LD. 2022. Production of large surface area activated carbon from a mixture of carrot juice pulp and pomegranate peel using microwave radiation-assisted ZnCl₂ activation: an optimized removal process and tailored adsorption mechanism of crystal violet dye. Diam Relat Mater. 130:109456. doi:10.1016/j.diamond.2022.109456.

Teow YH, Nordin NI, Mohammad AW. 2019. Green synthesis of palm oil mill effluent based graphenic adsorbent for the treatment of dye-contaminated wastewater. Environ Sci Pollut Res. 26(33):33747–33757. doi:10.1007/s11356-018-2189-6.

Veeraragavan AJ, Shanmugavel R, Abraham N, Subramanian D, Pandian S. 2021. Kinetic studies validated by artificial neural network simulation for the removal of dye from simulated waste water by the activated carbon produced from Acalypha indica leaves. Environ Technol Inno. 21:101244. doi:10.1016/j.eti.2020.101244.

Wang S, Li L, We H, Zhu ZH. 2005. Unburned carbon as a low cost adsorbent for treatment of methylene blue containing wastewater. J Colloid Interface Sci. 292(2):336–343. doi:10.1016/j.jcis.2005.06.014.

Wannahari R, Sannasi P, Nordin MFM, Mukhtar H. 2018. Sugarcane bagasse-derived nano-magnetic adsorbent composite (SCB-NMAC) for removal of Cu^{+2} from aqueous solution. ARPN J Eng Appl Sci. 13(1):1–9.

Yaseen DA, Scholz M. 2019. Textile dye wastewater characteristics and constituents of synthetic effluents: a critical review. Int J Environ Sci Technol. 16(2):1193–1226. doi:10.1007/s13762-018-2130-z.

Yousef TA, Sahu UK, Jawad AH, Malek NNA, Al Duaij OK, ALOthman ZA. 2022. Fruit peel-based mesoporous activated carbon via microwave assisted K₂CO₃ activation: box Behnken design and desirability function for methylene blue dye adsorption. Int J Phytoremediation. 1–13. Online ahead of print. doi:10.1080/15226514.2022.2137102.

Yuan D, Zhou L, Fu D. 2017. Adsorption of methyl orange from aqueous solutions by calcined ZnMgAl hydrotalcite. Appl Phys A Mater Sci Process. 123:1–8.

Zeng XK, Ye M, Burkardt J, Wu JC, Wang D, Zhu XB. 2016. Evaluating two sparse grid surrogates and two adaptation criteria for groundwater Bayesian uncertainty quantification. J Hydrol. 535:120–134. doi:10.1016/j.jhydrol.2016.01.058.